Morphogenetic and patterning defects explain the coloboma phenotype of the eye in the Mexican cavefish

Lucie Devos[1], Florent Klee[1], Joanne Edouard[2], Victor Simon[1,2], Laurent Legendre[2], Naima El Khallouki[2], Maryline Blin[1], Sosthène Barbachou[2], Frédéric Sohm[2] and Sylvie Rétaux[1]

[1] Paris-Saclay Institute of Neuroscience, CNRS UMR 9197, Université Paris-Saclay, 91198 Gif sur Yvette, France

[2] UMS AMAGEN, CNRS, INRA, Université Paris-Saclay, 91198, Gif sur Yvette, France

Key words (6): *Zic1*; CRISPR/Cas9 knock-in; *Astyanax mexicanus*; live imaging, retina patterning, retinal pigmented epithelium

Abstract

The morphogenesis of the vertebrate eye consists of a complex choreography of cell movements, tightly coupled to axial regionalization and cell type specification processes. Any disturbance in these events can lead to developmental defects and blindness. Here we have deciphered the sequence of defective events leading to coloboma phenotype in the embryonic eye of the blind cavefish of the species *Astyanax mexicanus*. Using comparative live imaging on targeted enhancer-trap *Zic1:hsp70:GFP* reporter lines of both the normal, river-dwelling morph and the cave morph of the species, we identified major defects in initial optic vesicle size and optic cup invagination in cavefish. Combining these results with gene expression analyses, we also discovered defects in axial patterning affecting mainly the temporal retina, in optic stalk tissue specification, and in the spreading processes involving the retinal pigmented epithelium cells. Based on these results, we propose a developmental scenario to explain the cavefish phenotype and discuss developmental constraints to morphological evolution. The cavefish eye appears as an outstanding natural mutant model to study molecular and cellular processes involved in optic region morphogenesis.

Introduction

The morphogenesis of the vertebrate eye is a complex choreography of cell movements starting from a flat neural plate and leading to the formation of a spherical multi-layered structure. Owing to technological improvements, this process has been increasingly investigated in the last decade, especially on teleost models which are amenable to live imaging due to their external development and transparency (England et al., 2006; Ivanovitch et al., 2013; Kwan et al., 2012; Martinez-Morales et al., 2009; Nicolas-Perez et al., 2016; Picker et al., 2009; Rembold et al., 2006; Sidhaye and Norden, 2017). This focus on morphogenesis led to the description of cell and tissue movements during eye development in fish (reviewed in Cavodeassi, 2018) (**Fig. S1**).

At the end of gastrulation, the eyefield is specified in the anterior neural plate, surrounded anteriorly and laterally by the prospective telencephalon, and posteriorly by the future hypothalamus and diencephalon (Varga et al., 1999; Woo and Fraser, 1995; Woo et al., 1995). During neurulation, the first step of eye formation is the lateral evagination of the optic vesicles. Already at this step, cell behaviours are complex as some eye-fated cells behave like the nearby telencephalic cells and converge toward the midline to form the neural keel, while others lag behind and keep the eyefield wide (Ivanovitch et al., 2013; Rembold et al., 2006). The eye vesicles then elongate due to a flow of cells entering the anterior/nasal optic vesicle, in a process recently re-described as “extended evagination” (Kwan et al., 2012). Simultaneously, the optic vesicles are separated from the neural keel by the anterior-wards progression of a posterior furrow between them and the diencephalon, leaving a connection with the neural tube at the optic stalk (England et al., 2006). Cells from the medial part (inner leaflet) of the optic vesicle then migrate around the rim of the eye ventricle (the optic recess) into the lens facing neuroepithelium through a process called rim movement (Heermann et al., 2015; Kwan et al., 2012). The cells in the outer layer of the optic cup, fated to the retinal pigmented epithelium (RPE), expand and flatten to cover the back of the retina (Cechmanek and McFarlane, 2017; Heermann et al., 2015). Together with the basal constriction of lens-facing epithelial cells (Martinez-Morales et al., 2009; Nicolas-Perez et al., 2016), these movements lead to optic cup invagination. The invagination process leads to the formation of

70 the optic fissure at the level of the connection of the eye with the optic stalk. This fissure
71 allows bloods vessels to invade the eye and leads the way of retino-fugal axons, but needs to
72 close to have a functional and round eye (Gestri et al., 2018). Finally, the entire eye, together
73 with the forebrain, rotates anteriorly, bringing the optic fissure in its final ventral position.
74 Hence, cells that are initially located in the dorsal or ventral part of the optic vesicles
75 contribute to the nasal or temporal quadrant of the retina, respectively (Picker et al., 2009).
76 Failure to correctly complete any of these steps can lead to vision defects; for example, failure
77 to properly close the optic fissure is termed coloboma and can lead to congenital blindness.

78 During the eye morphogenetic process, three types of tissues emerge: (1) the neural retina,
79 facing the lens and composed of various neuronal types, (2) the RPE at the back of the neural
80 retina, with multiple functions including nurturing of photoreceptors (Strauss, 2018), and (3)
81 the optic stalk, transiently connecting the retina to the neural tube. This thin ventral structure
82 is invaded by the ganglionic cells axons and guides them on their way to the tectum. Optic
83 stalk cells then differentiate into reticular astrocytes surrounding the optic nerve (Macdonald
84 et al., 1997). All these tissues derive from the optic vesicles and have a neural origin.

85 Concomitantly to morphogenesis, retinal cells acquire axial positional identity. Indeed, the
86 visual sense requires a topographic perception of the light stimuli and processing of the signal
87 to form images. In fishes, the neuronal map of the retina is replicated onto the contralateral
88 tectum, in a symmetrical manner so that the nasal retina projects to the posterior optic
89 tectum, while the temporal retina projects to the anterior tectum. This retinotopy requires a
90 precise regional identity of both the retina and the tectum for a proper matching (Rétaux and
91 Harris, 1996; Sperry, 1963). In the retina, several transcription factors such as *Vax2*, *FoxG1*,
92 *Tbx5a*, or *FoxD1* present a strong regional expression, already present at optic vesicle stage,
93 and define the future quadrants identity by controlling the expression of effector guidance
94 molecules (French et al., 2009; Picker et al., 2009; Sakuta et al., 2006; Schulte et al., 1999). The
95 regionalized expression of the transcription factors themselves is mainly achieved through
96 Hedgehog and Fgf signalling from the embryonic midline, and reciprocal interactions between
97 them (Asai-Coakwell et al., 2007; Hernandez-Bejarano et al., 2015; Kruse-Bend et al., 2012;
98 Picker and Brand, 2005; Picker et al., 2009). Shh is involved in the regulation of the ventral and
99 temporal fates while Fgfs secreted by the anterior neural ridge and olfactory placode seem to
100 be involved in nasal specification. Extra-ocular Bmps direct the acquisition of dorsal fates

101 (Gosse and Baier, 2009; Hernandez-Bejarano et al., 2015; Picker and Brand, 2005; Picker et al.,
102 2009; Take-uchi et al., 2003).

103 *Astyanax mexicanus* is a teleost fish that arises in two morphs: the classical river-dwelling eyed
104 morph and the cave-dwelling blind morph. Although eyes are absent in adult cavefish, they
105 first develop in embryos before degenerating during larval stages. The early cavefish eyes
106 display several morphogenesis abnormalities: the optic vesicles are short (Alunni et al., 2007),
107 the optic cup and lens are small (Hinaux et al., 2015; Hinaux et al., 2016; Yamamoto and
108 Jeffery, 2000) and the ventral part of the optic cup is severely reduced or lacking, leaving the
109 optic fissure wide open (coloboma phenotype) (Pottin et al., 2011; Yamamoto et al., 2004).
110 Moreover, cavefish exhibit several modifications of morphogen expression including an
111 expanded *Shh* expression at the anterior midline, a heterochrony of *Fgf8* onset in the anterior
112 neural ridge, and variations of *Bmp4* and *Dkk1b* expression in the prechordal plate (Hinaux et
113 al., 2016; Pottin et al., 2011; Torres-Paz et al., 2018; Yamamoto et al., 2004). These morphogen
114 alterations trigger modifications of the cavefish eyefield and subsequent eye, as evidenced by
115 modified expression of *Lhx9/2* or *Pax6* in the neural plate when compared to surface fish
116 embryos (Pottin et al., 2011; Yamamoto et al., 2004), and they have been linked to cavefish
117 eye development defects: overexpression of *Shh* in surface fish shortens its optic cups and
118 triggers the apoptosis of the lens, while inhibition of Fgf signalling in a cavefish restores the
119 ventral retina (Hinaux et al., 2016; Pottin et al., 2011; Yamamoto et al., 2004).

120 Because of these various modifications, the cavefish is a remarkable natural mutant model to
121 study eye development, beyond the mechanisms of eye degeneration and loss. We therefore
122 undertook to study the morphogenesis and regionalization of the cavefish eye, in comparison
123 with surface fish, with two aims: a better understanding of the defects of the cavefish
124 embryonic eye as well as the mechanisms of eye morphogenesis in general.
125

126 Using CRISPR/Cas9-mediated targeted enhancer trap cavefish and surface fish *Zic1:hsp70:GFP*
127 lines, we performed comparative live imaging of eye morphogenesis on developing embryos.
128 We propose that the reduction in cavefish optic vesicle size, associated with a proper
129 extended evagination, leads to a bias towards nasal fate and an abnormal final ventral position
130 of the lens. In addition, optic cup invagination is impaired and RPE spreading over the surface
131 of the neural retina is delayed in cavefish. Through gene expression analyses, we show

moreover that the cavefish eyes display modifications of their axial regionalization, with a tendency to preserve or increase nasal and dorsal fates while strongly diminishing temporal fate. Finally, the optic stalk fate is widely increased throughout the retina.

136 # Results

137

138 **Screening candidate genes to establish *Astyanax* GFP reporter lines**

139 To perform live imaging and label regions of interest, i.e. the entire optic region of cavefish
140 (CF) and surface fish (SF) embryos, we sought to find a reporter gene that would be expressed
141 in the eyefield from the neural plate stage (10hpf) until at least 24 or 36hpf, when optic recess
142 region (ORR) and retina are clearly separated (Affaticati et al., 2015). An *in situ* hybridization
143 mini-screen for candidate genes selected from publications and the ZFIN expression database
144 was performed. Chosen candidates were *Vax1*, *Vax2* (Take-uchi et al., 2003), *Zic1* (Hinaux et
145 al., 2016; Maurus and Harris, 2009; Rohr et al., 1999; Tropepe et al., 2006), *Zic2a* (Sanek et al.,
146 2009), *Rx3* (Deschet et al., 1999; Rembold et al., 2006; Stigloher et al., 2006), *Lhx2* and *Lhx9*
147 (Pottin et al., 2011). We performed *in situ* hybridization on CF and SF embryos at 5 different
148 stages (10, 12, 14, 24 and 36hpf) (**Fig. S2A**).

149 Among the 7 genes, 5 were expressed in the anterior neural plate at 10hpf while 2 were not:
150 *Vax1* and *Vax2*, whose expressions were detectable from 12hpf only (**Fig. S2A**). Five of them
151 were expressed at least partially in the optic vesicle per se (excluding ORR and optic stalk):
152 *Vax2*, *Zic1*, *Rx3*, *Lhx9* and *Zic2a* (faintly). At 36hpf, only 4 of them were still expressed in the
153 optic cup: *Zic2a* and *Zic1* (around the lens), *Lhx2* (faintly) and *Vax2* (in the ventral retina).
154 Subtle differences between CF and SF expression patterns were observed (not shown), and
155 only one candidate genes was consistently expressed in the eye from neural plate to 36hpf:
156 *Zic1* (**Figure 1A** and **Fig. S2B**; see legend of **Fig. S2B**). Even though the *Zic1* pattern was complex
157 and encompassed a region wider than the optic region of interest, it was chosen for
158 transgenesis due to its early and persistent expression throughout the eye and the ORR/optic
159 stalk regions.

160

161 **Comparative expression of *Zic1* in surface fish and cavefish embryos**

162 A closer examination of *Zic1* pattern highlighted some patterning and morphological
163 differences between SF and CF (**Figure 1A**). In the anterior neural plate at 10hpf, *Zic1*
164 expression was wide in the bilateral eyefield in SF, with a medial indentation (**Figure 1A**,

165 asterisk); in CF, *Zic1* was expressed in narrower lateral bands, with a wider staining anteriorly.
166 At 12hpf, *Zic1* pattern confirmed that the CF optic vesicles were shorter than those of SF, but
167 they also looked more "plump". Indeed, from a dorsal view SF optic vesicles were elongated,
168 slender and pointier while CF optic vesicles looked rounder. On lateral views, the optic vesicles
169 showed a trapezium shape in SF and an oval shape in CF. At 36hpf the *Zic1*-expressing ORR
170 was wider in cavefish. These differences in expression patterns decisively convicted us to use
171 *Zic1* as reporter gene.

172

173 **Establishing *Zic1:hsp70:GFP* surface fish and cavefish knock-in lines**

174 We used a targeted enhancer-trap strategy into the *Zic1* locus to generate reporter lines. This
175 option presented the advantage that the GFP reporter insertion site would be identical in CF
176 and SF lines and avoid positional effects, which is crucial for comparative purposes. The
177 genomic region around *Zic1* was examined to find conserved elements that might point
178 toward putative regulatory elements (**Fig. 1BC**). The region was large (~500 kb in zebrafish)
179 and complex. In the zebrafish genome which has a better quality and annotation than the
180 *Astyanax* genome (McGaugh et al., 2014), *Zic1* and *Zic4* were very close to each other in a
181 head to head configuration, and located in the middle of a gene desert (~200kb downstream
182 of *Zic1* and ~220kb downstream of *Zic4* in zebrafish, and ~275kb downstream of *Zic1* and
183 ~235kb downstream of *Zic4* in *Astyanax)*. This gene desert contained many elements
184 conserved among fishes, also partly conserved with tetrapods and mammals (**Fig. 1BC**). Such
185 a regulatory landscape suggested that the elements driving *Zic1* expression are probably
186 modular and difficult to identify, further strengthening the choice of a directed enhancer-trap
187 approach.

188 Cavefish and surface fish embryos were co-injected with sgRNA2 (targeting the region
189 between conserved non-coding elements 1 and 2), Cas9 protein and a linearized minimal
190 promoter *hsp70:GFP* repair construct and were screened at 30hpf for fluorescence patterns
191 consistent with *Zic1* endogenous pattern (**Fig. 1CD**). Excellent *Zic1* pattern recapitulation in F0
192 was observed at low frequency (1-2% of injected embryos), while other more partial patterns
193 were also seen at higher frequencies. All potential founder embryos were sorted and raised
194 until males were sexually mature (5-6 months' post-fertilization) and could be screened by
195 individual *in vitro* fertilization. We detected 3 founders for SF (out of 15 F0 males screened)

196 and 5 founders for CF (out of 9 F0 males screened) with various transmission rates: 4%, 7%
197 and 30% for SF founders and 4%, 45%, 48%, 50% and 54% for CF founders, respectively. The
198 fish were screened based on their GFP pattern, matching *Zic1* (**Fig. 1D**). In both morphs some
199 variations in relative intensities of fluorescence were observed, with some lines exhibiting
200 more homogeneous levels of expression and others having an extremely strong GFP
201 fluorescence in the telencephalon and a dimer fluorescence in the eye. We focused on the
202 most homogeneous lines for imaging purposes. Importantly, in those lines, genomic analyses
203 confirmed the proper insertion of the transgene at the exact targeted site (**Fig. S3**), and double
204 fluorescent *in situ* hybridisation for *Zic1* and *GFP* mRNAs demonstrated that the reporter fully
205 recapitulated the endogenous *Zic1* pattern at the stages of interest (**Fig. 1E**).

206

207 **Comparing eye morphogenesis in surface fish and cavefish through live imaging**

208 Live imaging was performed on a light-sheet microscope on both CF and SF lines from ~10.5hpf
209 to 24-30hpf, depending on the acquisitions (**Fig. 2** and **Movies 1 and 2**). The planes used for
210 analysis were chosen to always cross the middle of the lens and the optic stalk (see drawings
211 on **Fig. 2**), in order to follow the anterior rotation of the eye. Overall, eye morphogenesis in SF
212 recapitulated step by step the events described in zebrafish, while in CF the morphogenetic
213 movements were conserved but their relative timing and extent seemed different. The
214 following analyses result from quantifications made on 4 eyes for each morph.

215

216 **Evagination and elongation.** The CF optic vesicles were much shorter from the beginning of
217 evagination onwards and they spanned about half the length of the SF optic vesicles at the
218 same stage (139µm compared to 216µm at 11.5hpf) (**Fig. 2A,B** and **Fig. 3A,B**). Elongation then
219 proceeded at approximately the same pace as in SF until 17.5hpf (**Fig. 3B**). However, while the
220 length of the eye primordium decreased between 17.5hpf and 25.5hpf in SF, due to the
221 invagination movement, elongation continued at slower pace until 25.5hpf in CF. Hence, the
222 increase in length from 11.5hpf (beginning of the furrow progression to separate the optic
223 vesicles from the neural tube in both morphs) to 31.5hpf was more important in CF than in SF,
224 because it remained flatter (**Fig. 3B**). Moreover, the final size of the SF optic cup was very
225 similar to that of its early evaginating eyefield (252µm at 31.5hpf compared to 240µm at

226 10.5hpf) while in CF a net increase in the optic primordium size was visible (186µm at 31.5 hpf
227 compared to 146µm at 10.5hpf) (**Fig. 3A**). In addition, while in SF the optic vesicles stayed
228 closely apposed to the neural tube, in CF they first started growing away from the neural tube
229 before getting back closer between 18.5 and 21.5hpf (**Fig. 2B**). Finally, throughout
230 development, the width of the optic stalk (defined in its wide meaning as the connection
231 between the optic vesicle/cup and the neural tube) was similar in the two morphs despite an
232 initially smaller size in the CF due to the smaller optic vesicles (**Fig. S4**).

233

234 **Optic cup invagination and lens formation.** The posterior end of the optic vesicles started
235 curling back in both CF and SF around 15.5hpf, probably due to basal constriction. The lens
236 started being identifiable at 17.5hpf in both morphs (**Fig. 2B** and **movies 1 and 2**). At this stage,
237 the lens was in a central position with regard to the antero-posterior extension of the optic
238 vesicles, in both morphs (**Fig. 2B and 3D**). Then, in SF the invagination quickly brought closer
239 the two edges of the optic cup, in contact with the lens (**Fig. 2B** and **Fig. 3C**). In contrast,
240 despite initially harbouring a curvature typical of an invaginating optic cup, the edges of the
241 CF optic cup did not undergo the same change of form and stayed "flat", with an apparent
242 impairment of the rim movement in the posterior optic cup (**Fig. 2B**, **Fig. 3C and Movie 2**). In
243 fact, the CF optic vesicles continued to elongate while the lens remained static, therefore
244 seemingly shifting the lens position anteriorly (**Fig. 2B** and **Fig. 3D**). During this period, the
245 posterior part of the CF optic cup showed slow and reduced curling, which in some embryos
246 led to a separation of the posterior optic vesicle from the lens. Yet the posterior (prospective
247 dorsal) optic cup finally curved and contacted the lens (see progression, especially on the right
248 eye from 22.5hpf to 30.5hpf, **Movie 2**; **Fig. 2B** and **Fig. 3D**). However, the CF optic cup
249 remained shallower as its lens, albeit smaller, always bulged out while in SF the lens was
250 always contained inside of the optic cup curvature.

251 In sum, live-imaging experiments suggested that in CF (1) the optic vesicles were reduced in
252 size after the initial evagination, (2) elongation of the optic vesicle occurred properly, including
253 for the extended evagination, while (3) invagination was transiently compromised. We
254 reasoned that these impaired morphogenetic movements should impact the proper
255 patterning and regionalization of the CF retina.

256

257 **Comparing eye regionalization in surface fish and cavefish**

258 In order to label the different quadrants of the eye, four classical markers were chosen: *FoxG1*
259 for the nasal quadrant, *Tbx5a* for the dorsal quadrant, *FoxD1* as a temporal marker and *Vax2*
260 as a ventral marker spanning both the nasal and temporal sides of the optic fissure (**Fig. 4**).
261 The difficulty of comparing these quadrants between CF and SF resided in the difference of
262 morphology and size of their eyes. We therefore decided to measure different parameters
263 including angles of expression (taking as a reference the centre of the lens and the middle of
264 the optic fissure if needed) and gene expression areas (expressed either as absolute values or
265 as relative values normalized to eye size). Below the expression patterns of the four markers
266 are described in a clock-wise manner starting at the optic fissure.

267 The nasal marker *FoxG1* presented a larger angle of expression in CF (149°) than in SF (132°)
268 due to a dorsal expansion of the expression domain (**Fig. 4A-A''**). In CF the dorsal marker *Tbx5a*
269 started at the same angle from the optic fissure but spanned an increased angle towards the
270 temporal retina (angle to mid-fissure: 106° for SF and 111° for CF; span: 108° for SF and 139°
271 for CF) (**Fig. 4B-B''**). Reciprocally to these two increases of expression domains in the clock-
272 wise direction, the temporal marker *FoxD1* span was reduced in its dorsal part in CF (179° in
273 SF, 141° in CF) (**Fig. 4 C-C''**). Finally, the ventral marker *Vax2* had different features on the
274 nasal and temporal margins of the optic fissure. *Vax2* span was increased in the ventro-nasal
275 quadrant, indicating a dorsal-wards or clock-wise expansion (66° in SF, 94° in CF) while it was
276 unchanged in the temporal quadrant when compared to SF (**Fig. 4 D-D''**).

277 The smaller size of the CF eye was reflected by the absolute values of markers expression areas
278 (**Fig. 4E**). Indeed, all of them but one (*Tbx5a*) were decreased in size, including nasal *Vax2* and
279 *FoxG1* expression domains which were slightly but significantly reduced. *Tbx5a* was the only
280 gene showing the same area of expression in CF and SF eyes, suggesting that the dorsal
281 quadrant was proportionately increased in cavefish. The two temporal genes, *FoxD1* and *Vax2*,
282 exhibited a strong reduction of expression area, pointing to a temporal reduction in the
283 cavefish eye. This conclusion was further supported when the gene expression areas were
284 expressed in relative values normalized to eye size (**Fig. 4F**) or in percentages of SF labelling
285 (**Fig. 4G**). Indeed, the most strongly reduced quadrant was the temporal quadrant, labelled by
286 *FoxD1* and the temporal aspect of the *Vax2* domain.

287 Thus, in CF all markers examined presented modifications of expression in a fan-opening
288 fashion, from nasal towards temporal, overall increasing the nasal and dorsal fates at the
289 expense of the temporal retina. Contrarily to the usual description of the cavefish eye as
290 ventrally-reduced, we unmasked here a temporal reduction.

291

292 **Comparing tissue and cell identity markers in surface fish and cavefish**

293 To assess tissue identity in the developing retina, *Pax2a* was used as a marker for optic stalk
294 and optic fissure margin identity (Macdonald et al., 1997) and *Bhlhe40* (Cechmanek and
295 McFarlane, 2017) was used as a RPE identity marker.

296 *Pax2a* showed wider expression in cavefish, expanding beyond the optic fissure margins and
297 occupying a large part of the ventral quadrants both nasally (angles, SF: 36°, CF: 67°) and
298 temporally (angles, SF: 21°, CF: 55°) (**Fig. 5A-A''**). Surprisingly, in CF eyes *Pax2a* expression
299 sometimes expanded throughout the retina with a lighter, although specific, expression
300 intensity. Staining was even sometimes present in the dorsal quadrant, opposite to the optic
301 stalk or optic fissure margins without obvious staining in between (see **Fig. 5A'**). These
302 "dorsal" phenotypes were observed in 60% of CF embryos, but never in SF.

303 In 36hpf SF embryos the RPE marker *Bhlhe40* was expressed all around the eye, often
304 contacting the lens (4.7µm away) (**Fig. 5B, B', D**), which was taken as an indicator of the correct
305 engulfment of the retina by the migrating RPE. The edges of the optic fissure margins
306 sometimes lacked staining but overall the expression spanned 326° around the eye (**Fig. 5B''**).
307 Conversely, in CF, *Bhlhe40* expression area was reduced, with a wider ventral gap possibly
308 resulting from the wider optic fissure opening, and a significantly diminished covering of the
309 retina by the RPE (289° around the eye). *Bhlhe40*-positive cells were also found further away
310 from the lens (15µm), reinforcing the idea of a reduced retina covering by the RPE at this
311 stage; at 48hpf however, the staining span was increased and no longer significantly different
312 from the 36hpf SF (CF 48hpf: 309°; SF 36hpf: 326°) (**Fig. 5B, C, B''**). These data suggest a slower
313 but still occurring engulfment of the back of the retina by the RPE.

314 The back of the retina was usually well covered with *Bhlhe40*-expressing RPE cells, but with a
315 ventral gap which was well delimited by strongly contrasted, sharp edges (**Fig. S5**). We
316 interpreted this gap as the "exit point" of the optic stalk and used it as a proxy for optic stalk

317 width. The *Bhlhe40* gap was wider in CF than in SF (SF: 41µm, CF: 60µm) (**Fig. 5E**). This was
318 consistent with the above-reported increase in *Pax2a* expression domain and points towards
319 an increased optic stalk size in cavefish.

320 Altogether, these results suggested that both the RPE engulfment/spreading movement and
321 the optic fissure margins juxtaposition are slowed -but occur in a delayed manner- in cavefish.
322 Below these findings are discussed altogether with regards to earlier observations of eye
323 morphogenesis through live imaging.

324 # Discussion

325

326 ***Astyanax* knock-in reporter lines obtained by CRISPR/Cas9**

327 Several transgenesis techniques are available in zebrafish and have already been adapted to
328 *Astyanax*: a classical approach consists in cloning a promoter or regulatory element driving
329 the expression of a reporter or effector gene under its control, flanked with either transposons
330 or meganuclease cutting sites (Kawakami, 2005; Thermes et al., 2002). After injection with the
331 appropriate enzyme, transposase or meganuclease, into the 1st cell of the embryo, the
332 construct is randomly inserted one or several times in the genome. This method is technically
333 simple and works in *Astyanax* (Elipot et al., 2014; Hinaux et al., 2015; Stahl et al., 2019). It has
334 however several drawbacks: the correct identification of most if not all the regulatory
335 sequences driving expression is necessary and often difficult; the insertion of the transgene is
336 random and its expression depends on the insertion site; the insertion of the construct can
337 disrupt coding or regulatory sequences.

338 The advent of the flexible CRISPR/Cas9 technique now allows for an "easy" RNA-mediated
339 targeting at a precise genomic location. However, if performing a targeted knock-out by
340 cutting DNA and relying on the imprecise non-homologous end joining (NHEJ) DNA repair
341 mechanism to generate indels and frameshifts has proven quite efficient, more precise repair
342 and insertions are still difficult to obtain, at least in zebrafish. The more precise methods
343 require homology-directed repair and therefore involve homology arms flanking a repair
344 construct. Although different ways to increase homology-directed repair efficiency have been
345 tested (Albadri et al., 2017; Morita et al., 2017), it is still a very challenging method as NHEJ is
346 the preferred repair mechanism in fish embryos (Hagmann et al., 1998).

347 The difficulty of identifying *Zic1* regulatory elements with comparative genomics led us to
348 adopt a targeted enhancer-trap strategy, using a NHEJ DNA repair mechanism-based approach
349 to maximize integration efficiency. This option also had the advantage that the insertion site
350 would be similar in CF and SF lines, which is crucial for comparative purposes. Enhancer traps
351 were originally performed by random insertions in a two-step process, the first step being the
352 selection of the expression pattern of interest, the second the identification of the region in

353 which the transgene was inserted. This allowed the generation of transgenic lines with various
354 patterns of expression, reflecting the activity of one or more enhancers and regulatory
355 elements. Here, we "addressed" the enhancer-trap construct to *Zic1* downstream genomic
356 region using CRISPR/Cas9 methodology, similarly to what was performed by Kimura and
357 colleagues (Kimura et al., 2014). This method yielded good results as its limited efficiency was
358 compensated by the possibility of using a pattern-based fluorescence screening in F0
359 embryos. Hence, we obtained an excellent ratio of founder fish in the pool of selected F0
360 embryos (more than 50% in cavefish). Finally, for both morphs the different *Zic1:hsp70:GFP*
361 lines, although recapitulating the *Zic1* pattern, showed slight variations in the relative
362 intensities of reporter fluorescence in the telencephalon and in the eyes. The insertion
363 method being based upon non conservative NHEJ mechanism, those variations are likely due
364 to sequence differences from one line to the next (indels and duplications in the genomic DNA
365 or the transgene), which may affect the nearby regulatory sequences and slightly modify
366 transgene expression. However, those variations remain anecdotal compared to the
367 differences observed between lines generated by traditional transgenesis techniques (such as
368 Tol2 promoter transgenesis), validating this approach as a tool to follow gene expression in
369 *Astyanax* morphotypes.

370 CRISPR/Cas9 has been previously reported in surface *Astyanax mexicanus* to generate an *Oca2*
371 null mutant and confirm the role of *Oca2* in the control of pigmentation (Klaassen et al., 2018).
372 But this is to our knowledge the first report of the CRISPR/Cas9 technology used in this
373 emergent model species to generate identical reporter lines in the two morphotypes, and in
374 a targeted genome edition perspective.

375

376 **Live imaging**

377 The choice of live imaging microscopy technique was directed by several parameters, from
378 the intensity of the labelling to temporal-spatial resolution trade-off. Light-sheet or SPIM
379 (single plane illumination microscopy) microscopy offered several advantages such as wide
380 dynamic range of the camera, allowing to detect both the strong labelling of the telencephalon
381 and the fainter labelling of the eye. The next step of this study will be to track the cells
382 participating in the formation the optic region, i.e. eye, optic stalk, ORR. Cells in these regions

383 undergo fast movements during early morphogenesis, so that a good time resolution is
384 necessary. They are also densely-packed and therefore require a good spatial resolution.
385 Moreover, live embryos are fragile and laser power must be kept minimal to avoid bleaching
386 of the fluorescence and photo-damage. In contrast to the point acquisition of the confocal
387 microscope, the plane acquisition of the SPIM allowed fast imaging while retaining sufficient
388 spatial resolution. The orthogonal illumination induced minimal photo-damage and embryos
389 developing for more than 20 hours under the microscope recovered well and were alive with
390 a normal head shape at 48-60hpf -even though the tail was usually twisted due to the
391 mechanical constraint in the low-melting agarose.

392

393 **Recapitulating cavefish eye development**

394 Live imaging performed on the *Zic1:hsp70:GFP* transgenic lines combined to gene expression
395 studies allowed us to reveal striking differences in eye morphogenesis, morphology and
396 patterning between the two *Astyanax* morphs. Because the ventral quadrant of the eye was
397 originally described as reduced and because the expression of the ventralizing morphogen Shh
398 was known to be enlarged in cavefish (Yamamoto et al., 2004), we expected a global
399 "ventralization" of the eye quadrants at the expense of the dorsal quadrant which we assumed
400 would be reduced. However, the data revealed a quite different story and we venture to
401 propose a developmental scenario for cavefish morphogenesis and patterning (**Fig. 6**).

402 (1) First, the shorter size of the cavefish optic vesicles (Alunni et al., 2007; Strickler et al., 2001)
403 seems principally due to the smaller eyefield, since elongation proceeds similarly in CF and SF
404 until 17.5hpf. Increased Hedgehog signalling in CF was shown to decrease the size of its optic
405 vesicles (Yamamoto et al., 2004) and probably the eyefield size, which could account for the
406 final smaller eye size. Moreover, albeit smaller, CF optic vesicles are "correctly" patterned in
407 their future naso-temporal axis, as shown by Hernández-Bejarano and colleagues at 10/12
408 somite stage (~13.5hpf) using *FoxG1* and *FoxD1* markers (**Fig. 6A**) (Hernandez-Bejarano et al.,
409 2015).

410 (2) Second, after the initial evagination and patterning of a small optic vesicle, morphogenesis
411 proceeds with the "extended evagination", whereby cells from the neural tube continue
412 entering the optic vesicle to contribute exclusively to the ventro-nasal part of the eye (Kwan

413 et al., 2012). If this step proceeds normally in CF, which seems to be the case from live imaging
414 experiments, it could partially compensate the originally small size of the eyefield/optic
415 vesicle, but only in the nasal part, while the temporal part would remain fully affected (**Fig.**
416 **6B**). This would well explain the increased angles of nasal *FoxG1* and *Vax2* expression in
417 comparison to the reduced temporal *FoxD1* and *Vax2* territories we observed. It is also worth
418 noting that early Hedgehog signalling can increase *Vax2* expression (before early optic vesicle
419 stage) in *Xenopus* (Wang et al., 2015), which could further explain *Vax2* nasal expansion.

420 (3) Third, the lens forms correctly at the centre of the optic vesicle in both morphs, in a proper
421 place with regard to the initial invagination of the optic cup; it is only at later stages that the
422 lens appears more anterior (i.e., facing the presumptive ventral retina after final eye rotation)
423 in cavefish. This apparent displacement of the lens relative to the retina is not due to a
424 movement of the lens -which remains fixed throughout eye morphogenesis, attached to the
425 overlying ectoderm from which it delaminates around 22hpf in *Astyanax* (Hinaux et al., 2017)-
426 but rather to a persistent elongation of the optic vesicle. This suggests normal interactions
427 between the optic vesicle and the lens to adjust their relative position and initiate optic cup
428 invagination. Indeed, in chick, the pre-lens ectoderm is required for normal optic cup
429 invagination while the lens placode itself is dispensable (Hyer et al., 2003). In cavefish such
430 mechanisms could exist and correctly initiate optic cup folding. Finally, the anterior-shifted
431 position of the lens, due to elongation of the cavefish optic vesicle without invagination,
432 explains why the lens is ventrally displaced in the mature eye: the final anterior rotation
433 movement brings it in a ventral position (**Fig. 6C**).

434 (4) Fourth, although the invagination of the CF optic vesicle seems to start normally between
435 15.5 and 19.5hpf, it only progresses very little afterwards so that the optic cup remains shallow
436 and elongated. This timing is very reminiscent of the 2 described steps of optic cup
437 invagination: basal constriction initiating the primary folding between 18 and 20hpf in
438 zebrafish (18ss to 22ss), followed by the rim movement which brings the presumptive retina
439 from the inner optic vesicle leaflet into the lens-facing epithelium by an active migration
440 around the rims of the optic recess between 20 and 24hpf (Heermann et al., 2015; Nicolas-
441 Perez et al., 2016; Sidhaye and Norden, 2017). In *Astyanax*, 18 ss corresponds to ~16.5hpf
442 (Hinaux et al., 2011), suggesting that the initial basal constriction leading to the onset of optic
443 cup invagination is well conserved in cavefish –this will have to be confirmed. In contrast, the

444 prolonged extension of the optic vesicle and the fact that the curvature of the retina remains
445 shallow with the lens bulging out of the eye suggests that the rim movement must be impaired
446 in cavefish. We propose that the continuous flow of cells entering the retina leads to its
447 elongation, in the absence of an efficient rim movement. This movement does seem weaker
448 but not absent in CF, as the posterior part of its optic cup still manages to contact the lens,
449 but at later stages. This difference of rim movement might be due to various causes such as
450 defects in the basal membrane or failure to establish proper focal adhesion as seen in the
451 *ojoplano* medaka mutant (Martinez-Morales et al., 2009; Nicolas-Perez et al., 2016; Sidhaye
452 and Norden, 2017). Alternatively, the active migration described by Sidhaye and Norden could
453 be altered by extrinsic signals, as in BMP overexpression experiments where the cell flow
454 toward the lens-facing epithelium is reduced (Heermann et al., 2015). The various morphogen
455 modifications known in cavefish, and the fact that the ventral eye can be restored by delaying
456 the onset of the Fgf signalling in CF to match the SF scenario (Pottin et al., 2011), support this
457 possibility.

458 The "continuous extension of the optic cup with only little rim movement" hypothesis explains
459 cavefish phenotypes. It clarifies the ventral and "floating" position of the lens in the final eye,
460 without much contact with the edges of the retina. It also explains how grooves/folds in the
461 retina (typically between the dorsal and temporal quadrants) are sometimes formed (**Fig. S6**).

462 (5) Fifth, *Bhlhe40* expression reveals that RPE identity is maintained in the CF eye. Yet, the
463 expansion and engulfment movement that this tissue is supposed to achieve to reach the rim
464 of the retina and cover the whole retina is delayed compared to SF. In fact, this spreading and
465 migration of RPE cells is concomitant with the rim movement and may contribute to it as a
466 driving force (Cechmanek and McFarlane, 2017; Moreno-Marmol et al., 2018). This
467 observation reinforces the idea that the rim movement is impaired in cavefish. Potentially, the
468 RPE movement may also be involved in optic fissure closure, as suggested by the presence of
469 a coloboma upon impairment of the rim movement by *BMP4* overexpression in the optic
470 vesicle (Heermann *et al.*, 2015). Deficiency in this morphogenetic movement might participate
471 in the cavefish coloboma phenotype. Of note, the transplantation of a healthy SF lens into a
472 CF optic cup rescues the eye as a structure, i.e., prevents lens-induced degeneration, but does
473 not rescue the coloboma phenotype (Yamamoto and Jeffery, 2000). This is in agreement with

474 our findings showing that the improper closure of the optic fissure is autonomous to the CF
475 retinal tissues and results from defective morphogenetic movements.

476 (6) Sixth, in addition and concomitantly to impaired morphogenetic processes, morphogen
477 signalling modifications previously reported in cavefish might contribute to the axial
478 patterning variations observed. On the naso-temporal axis, there seems to be a slight increase
479 in *FoxG1* domain in the early optic vesicle (Hernandez-Bejarano et al., 2015), which may be
480 explained by the earlier onset of *Fgf8* expression in the cavefish anterior neural ridge (Pottin
481 et al., 2011), but also by the increase in size of the cavefish olfactory placodes which also
482 secrete Fgf24 (Hernandez-Bejarano et al., 2015; Hinaux et al., 2016). These Fgfs, along with
483 Fgf3 promote retinal nasal fate (Hernandez-Bejarano et al., 2015; Picker and Brand, 2005;
484 Picker et al., 2009), and may be responsible for the slight expansion of *FoxG1* expression in
485 cavefish, itself limited or counteracted by increased Shh signalling (Hernandez-Bejarano et al.,
486 2015). This might contribute to the importance taken by nasal fates relative to temporal fates
487 in cavefish. It may also account for the *Tbx5a* angle enlargement towards the temporal
488 quadrant. In fact, Fgf signalling has been shown to promote dorsal identity temporally, as
489 demonstrated by the temporal reduction of *Tbx5a* span and its nasal shift in *Fgf8* mutant
490 zebrafish (*Ace*) (Picker and Brand, 2005). Finally, besides Shh, Fgf and Bmp signalling, it is to
491 note that the mouse *Lrp6* insertional mutant displays microphthalmia and coloboma (Zhou et
492 al., 2008), and that zebrafish treated with the Wnt-βcat pathway activator LiCl have small eyes
493 (Shinya et al., 2000), therefore the modulations of canonical Wnt signalling observed in
494 cavefish (Torres-Paz et al., 2018) probably also impact the development of their eyes.

495 (7) *Pax2a* expression domain is increased at the expense of the *Pax6*-expressing part of the
496 eyefield at neural plate stage in CF (Yamamoto et al., 2004). Here we expand these results at
497 later stage and show that *Pax2a* is no longer confined to the optic stalk and optic fissure
498 margins but invades the ventral retina and even often, the dorsal retina. Contrarily to *Vax2*,
499 *Pax2a*/optic stalk identity is expanded in both temporal and ventral directions. This phenotype
500 is probably caused by the increase in Shh signalling in cavefish, as Shh injections in zebrafish
501 embryos or *Ptch1* (a negative regulator of Hedgehog pathway) loss of function in *blowout*
502 mutants cause very similar phenotypes with a larger optic stalk and an invasion of the ventral
503 retina by *Pax2a* expression (Lee et al., 2008). Nevertheless, the observation of cells with an
504 optic stalk identity in the cavefish dorsal retina was surprising, as in zebrafish, Shh signalling

505 maintains the optic stalk-retina interface through the regulation of *Vax* genes (Take-uchi et
506 al., 2003), and here we found that *Vax2* was mis-expressed in a much milder manner than
507 *Pax2a*. A possibility would be that these *Pax2a* "ectopic cells" stem from abnormal
508 morphogenetic movements that could not be traced in our study.

509

510 **Evolutionary considerations**

511 In all eyeless or eye-reduced cave vertebrates examined so far, initial eye development occurs,
512 including the evagination of optic vesicles and further morphogenetic steps (e.g., Durand,
513 1976; Stemmer et al., 2015; Wilkens, 2001). This represents an energetically-costly process for
514 embryos, raising the question of why would all these different species first develop eyes which
515 are after all fated to degeneration, and suggesting that initial eye development cannot be
516 circumvented (Rétaux and Casane, 2013). Our results help further refine the step(s) in eye
517 morphogenesis that are subjected to developmental constraint. Indeed, in cavefish, the
518 (small) eyefield is correctly specified and the evagination/elongation steps, which correspond
519 to cell movements leading to the sorting of retinal versus adjacent telencephalic, preoptic and
520 hypothalamic cells of the neural tube, occurs properly. It is only after the segregation between
521 these differently-fated cell populations that the cavefish eye morphogenesis starts going awry,
522 with a defective invagination process, that will soon be followed by lens apoptosis and the
523 subsequent progressive degeneration of the entire eye. Therefore, our data support the idea
524 that the first steps of eye development constitute an absolute developmental constraint to
525 morphological evolution. To the best of our knowledge, the closest to a counter-example is
526 the medaka mutant eyeless, a temperature-sensitive *rx3* mutant line in which optic vesicles
527 evagination does not occur. However, the homozygous eyeless fish either die after hatching
528 (Winkler et al., 2000) or, for the 1% which can be raised to adulthood in laboratory, are sterile
529 probably due to anatomical hypothalamic or hypophysis defects (Ishikawa et al., 2001), still
530 reinforcing the hypothesis of a strong developmental constraint.

531

532 **Conclusion**

533 This work proposes conclusions and hypotheses regarding defective cavefish eye
534 morphogenesis, and interprets cavefish eye development in the frame of the current

knowledge on the topic. Further analyses including the tracking, characterization and comparison of cell movements occurring in both morphs will refine the current scenario. For example, quantifying the extent of the rim movement, the curvature of the optic cup and the amount of cells entering the optic vesicle through time would be informative. These data also pave the way for experiments aiming at understanding the defective molecular or signalling mechanisms in cavefish eye morphogenesis, using the *Zic1:hsp70:GFP* knock-in lines.

541 # Methods

542

543 **Animals**

544 Laboratory stocks of *A. mexicanus* surface fish and cavefish were obtained in 2004 from the
545 Jeffery laboratory at the University of Maryland. The surface fish were originally collected
546 from San Solomon Spring, Texas and the cavefish are from the Pachón cave in Mexico. Surface
547 fish are kept at 26°C and cavefish at 22°C. Natural spawns are induced after a cold shock (22°C
548 over weekend) and a return to normal temperature for surface fish; cavefish spawns are
549 induced by raising the temperature to 26°C. Embryos destined for *in situ* hybridization were
550 collected after natural spawning, grown at 24°C and staged according to the developmental
551 staging table (Hinaux et al. 2011) and fixed in 4% paraformaldehyde. After progressive
552 dehydration in methanol, they were stored at -20°C. Embryos destined to transgenesis or live
553 imaging were obtained by *in vitro* fertilization. Embryos were raised in an incubator until 1
554 month post fertilization for the surface fishes and two month post fertilization for the cavefish.
555 They were kept at low density (15/20 per litre maximum) in embryo medium, in 1 litre plastic
556 tanks with a soft bubbling behind the strainer. Larvae were fed from day 5 with paramecium
557 and transitioned to artemia nauplii from day 10-15. Artemia were given twice a day except for
558 the weekends (once a day) and carefully removed afterward to avoid polluting the medium.
559 At least two thirds of the medium were changed every day and dead larvae removed. After
560 one month for the surface fish and two months for the cavefish, juveniles were taken to the
561 fish facility where they were fed dry pellets (Skretting Gemma wean 0.3) and quickly moved
562 to bigger tanks in order to allow their fast growth.

563 Animals were treated according to French and European regulations of animals in research.
564 SR' authorization for use of animals in research is 91-116, and Paris Centre-Sud Ethic
565 committee authorization numbers are 2012-52 and 2012-56.

566

567 ***In situ* hybridization**

568 Some cDNAs were available from our cDNA library : *Zic1* (FO290256), *Zic2a* (FO320762) and
569 *Rx3* (FO289986), *FoxD1* (FO380710); others were already cloned in the lab : *Lhx2* (EF175737)

570 and *Lhx9* (EF175738) (Alunni et al. 2007); obtained from other labs (*Vax1* : Jeffery lab,
571 University of Maryland,(Yamamoto et al. 2004)); or cloned for the purpose of this work in
572 pGEMT-Easy (Promega) :

573 • FoxG1: forward primer CTGACGTTCATGGACCGAGC; reverse primer
574 CAGTCTGCTTCCTGTGGATGT.
575 • Tbx5a: forward primer GCCTTCATTGCGGTCACTTC; reverse primer
576 CCCTCGTTCCATTCAGGCAT.
577 • Vax2: forward primer GGGCAAAACATGCGCGTTA; reverse primer
578 CAGTAATCCGGGTCCACTCC.
579 • Pax2a: forward primer AGCTGCATAACCGAGGCGA; reverse primer
580 CTCCATTAGAGCGAGGGATTCCGA
581 • Bhlhe40: forward primer : GCACTTTCCCTGCGGATTTC; reverse primer :
582 TGGAGTCTCGTTTGTCCAGC

583 cDNAs were amplified by PCR, and digoxygenin-labelled riboprobes were synthesized from
584 PCR templates. Embryos were rehydrated by graded series of EtOH/PBS, then for embryos
585 older than 24hpf, proteinase-K permeabilization at 37°C was performed for 36hpf embryos
586 only (10 µg/ml, 15 min) followed by a post-fixation step. Riboprobes were hybridized for 16
587 hr at 65°C and embryos were incubated with anti-DIG-AP (Roche, dilution 1/4000) overnight
588 at 4°C. Colorimetric detection with BCIP/NBT (Roche) was used. Mounted embryos were
589 imaged on a Nikon Eclipse E800 microscope equipped with a Nikon DXM 1200 camera running
590 under Nikon ACT-1 software. Brightness and contrast were adjusted using FIJI, some of the
591 images used for illustration purpose were created from an image stack, using the extended
592 depth of field function of Photoshop CS5. Area, distance and angle measurements were
593 performed using FIJI (Schindelin *et al.*, 2012; Schneider, Rasband and Eliceiri, 2012).

594

595 **In vitro fertilization (IVF) and injections**

596 Surface and cavefish were maintained in a room with shifted photoperiod (light: 4pm – 7am,
597 L:D 15:11) in order to obtain spawns during the working day (*Astyanax* spawn at night (Simon
598 et al., 2019)). Fish activity was monitored after induction and upon visible excitation or when
599 first eggs were found at the bottom of the tank, fish were fished. Females were processed first

600 to obtain eggs: they were quickly blotted on a moist paper towel and laid on their side in a
601 petri dish. They were gently but firmly maintained there while their flank was gently stroked.
602 If eggs were not released immediately, the female was put back in the tank. Once eggs were
603 collected, a male was quickly processed similarly to females, on the lid of the petri dish to
604 collect sperm. The sperm was then washed on the eggs with 10-20mL of tank water
605 (conductivity ~500µS) and left for a few moments (30s to 2 min approximatively), after which
606 embryo medium was added in the petri dish. Fertilised eggs were quickly laid on a zebrafish
607 injection dish containing agarose grooves. They were injected with a Picospritzer III (Parker
608 Hannifin) pressure injector.

609

610 **CRISPR injections and Knock-In lines**

611 sgRNA were designed to target the low-conservation regions between elements 1 and 2 and
612 between elements 3 and 4. Two sgRNA were initially designed per region and sgRNA2 was
613 found to efficiently cut the targeted region (**Fig. S7)**. The mix contained Cas9 protein
614 generously provided by TACGENE and sgRNA2 with the following targeting sequence:
615 CCCAATTCACCAGTATACGT (synthesized with AMBION T7 MEGAshortscript™ T7 transcription
616 kit). Concentrations were kept with a 1:1.5 Cas9 to sgRNA molar ratio and varied between
617 0.71µM (25ng/µL) and 5.67µM (200ng/µL) of sgRNA 2, mostly 2.84 and 1.42µM were used.
618 The donor construct contained a HSP70 promoter used as a minimal promoter, a GFP cDNA
619 and SV40 poly-adenylation signal, flanked by I-SceI meganuclease cutting sites. I-SceI was used
620 to generate sticky ends and was either detached by 7 min at 96°C or injected with the
621 construct. Concentrations of the repair construct varied between 3.33 and 10.92nM but were
622 mostly used at 10.71nM.

623

624 **mRNA injection**

625 Transgenic embryos used for live imaging were injected in the cell or yolk at 1 cell stage with
626 a H2B-mCherry fusion mRNA at a concentration of 50ng/µL.

627

628 **Imaging**

629 Transgenic embryos were obtained by IVF with wild-type eggs and transgenic sperm and were
630 immediately injected with H2B-mCherry mRNA for nuclear labelling. Injected embryos were
631 screened for GFP and mCherry fluorescence under a Leica M165C stereomicroscope around
632 10-11hpf, when GFP reporter fluorescence first becomes detectable.

633 Selected embryos were immediately mounted in a phytagel tube (SIGMA, CAS Number:
634 71010-52-1) molded with Phaseview Teflon mold (1.5mm of diameter) and maintained in
635 position with 0.4% low melting point agarose (Invitrogen UltraPure™ Low Melting Point
636 Agarose). The tube containing the embryo was placed horizontally into the chamber
637 containing 0.04% Tricaine in embryo medium (Sigma, CAS Number: 886-86-2). The tube was
638 rotated under the microscope so that the embryo would face the objective.

639 Live imaging was performed approximately from 10.5-11hpf to 24hpf every 2.5min-3min,
640 using a Phaseview Alpha^3 light sheet apparatus, coupled with an Olympus BX43 microscope
641 and using either a 20X/NA 0.5 Leica HCX APO objective or a 20X/NA 0.5 Olympus objective.
642 Images were acquired using QtSPIM software (Phaseview), which controlled a Hamamatsu
643 ORCA-Flash4.0 Digital sCMOS camera.

644 Room temperature was maintained at 24°C by air conditioning and the chamber temperature
645 was further controlled by a BIOEMERGENCES-made thermostat. Medium level was
646 maintained by a home-made perfusion system and an overflow to renew the medium.

647

648 **Imaging analysis**

649 Images obtained were visualized with Arivis Vision4D software and re-oriented to adopt a
650 similar optical section plane, cutting through the middle of the lens and the optic stalk at all
651 time-steps. On one time-step per hour, measurements were performed on the re-oriented
652 image: optic vesicle/optic cup length (at the widest), optic vesicle size increase (calculated by
653 subtracting the length at the onset of furrow formation to the length at time t), optic stalk
654 width, distance between the anterior optic cup and the lens, distance between the posterior
655 optic cup and the lens, distance between the optic cup edges, position of the lens relative to
656 anterior optic vesicle (=distance between center of the lens and anterior OV / (distance
657 between center of the lens and anterior OV + distance between center of the lens and
658 posterior OV)) (see schemes on Figures).

Acknowledgements

Work supported by an Equipe FRM grant (DEQ20150331745) and an UNADEV/AVIESAN grant to SR. We thank Jean-Paul Concordet and Anne De Cian (Tacgene, Sorbonne Universités, Paris) for sharing Cas9 protein; Diane Denis, Krystel Saroul, Jocelyne Gaget, the Amagen personnel and the people from the fish facility for advices and care of our *Astyanax* colony; Patrick Para for making custom tools for live microscopy; Adeline Boyreau, Adeline Rausch, Fanny Husson, Elena Kardash and Nadine Peyrieras (BioEmergence platform, Gif sur Yvette, France) for reagents, discussions and advices on live imaging, and for the use of the SPIM and image analysis tools; Cyprian Wozniak, Arthur Le Bris and Gaël Launay from PhaseView (Verrière-le-Buisson, France) for technical support and development of tools on the light-sheet microscope; and François Agnès for scientific discussions.

References

Affaticati, P., Yamamoto, K., Rizzi, B., Bureau, C., Peyrieras, N., Pasqualini, C., Demarque, M. and Vernier, P. (2015). Identification of the optic recess region as a morphogenetic entity in the zebrafish forebrain. *Sci Rep* **5**, 8738.

Albadri, S., Del Bene, F. and Revenu, C. (2017). Genome editing using CRISPR/Cas9-based knock-in approaches in zebrafish. *Methods* **121-122**, 77-85.

Alunni, A., Menuet, A., Candal, E., Penigault, J. B., Jeffery, W. R. and Rétaux, S. (2007). Developmental mechanisms for retinal degeneration in the blind cavefish Astyanax mexicanus. *J Comp Neurol* **505**, 221-33.

Asai-Coakwell, M., French, C. R., Berry, K. M., Ye, M., Koss, R., Somerville, M., Mueller, R., van Heyningen, V., Waskiewicz, A. J. and Lehmann, O. J. (2007). GDF6, a novel locus for a spectrum of ocular developmental anomalies. *Am J Hum Genet* **80**, 306-15.

Cavodeassi, F. (2018). Dynamic Tissue Rearrangements during Vertebrate Eye Morphogenesis: Insights from Fish Models. *J Dev Biol* **6**.

Cechmanek, P. B. and McFarlane, S. (2017). Retinal pigment epithelium expansion around the neural retina occurs in two separate phases with distinct mechanisms. *Dev Dyn* **246**, 598-609.

Deschet, K., Bourrat, F., Ristoratore, F., Chourrout, D. and Joly, J. S. (1999). Expression of the medaka (Oryzias latipes) Ol-Rx3 paired-like gene in two diencephalic derivatives, the eye and the hypothalamus. *Mech Dev* **83**, 179-82.

Durand, J. P. (1976). Ocular development and involution in the European cave salamander, Proteus anguinus laurenti. *Biol Bull* **151**, 450-66.

Elipot, Y., Legendre, L., Père, S., Sohm, F. and Rétaux, S. (2014). Astyanax transgenesis and husbandry: how cavefish enters the lab. *Zebrafish* **11 (4)**, 291-299.

England, S. J., Blanchard, G. B., Mahadevan, L. and Adams, R. J. (2006). A dynamic fate map of the forebrain shows how vertebrate eyes form and explains two causes of cyclopia. *Development* **133**, 4613-7.

French, C. R., Erickson, T., French, D. V., Pilgrim, D. B. and Waskiewicz, A. J. (2009). Gdf6a is required for the initiation of dorsal-ventral retinal patterning and lens development. *Dev Biol* **333**, 37-47.

Gestri, G., Bazin-Lopez, N., Scholes, C. and Wilson, S. W. (2018). Cell Behaviors during Closure of the Choroid Fissure in the Developing Eye. *Front Cell Neurosci* **12**, 42.

Gosse, N. J. and Baier, H. (2009). An essential role for Radar (Gdf6a) in inducing dorsal fate in the zebrafish retina. *Proc Natl Acad Sci U S A* **106**, 2236-41.

Hagmann, M., Bruggmann, R., Xue, L., Georgiev, O., Schaffner, W., Rungger, D., Spaniol, P. and Gerster, T. (1998). Homologous recombination and DNA-end joining reactions in zygotes and early embryos of zebrafish (Danio rerio) and Drosophila melanogaster. *Biol Chem* **379**, 673-81.

Heermann, S., Schutz, L., Lemke, S., Krieglstein, K. and Wittbrodt, J. (2015). Eye morphogenesis driven by epithelial flow into the optic cup facilitated by modulation of bone morphogenetic protein. *Elife* **4**.

Hernandez-Bejarano, M., Gestri, G., Spawls, L., Nieto-Lopez, F., Picker, A., Tada, M., Brand, M., Bovolenta, P., Wilson, S. W. and Cavodeassi, F. (2015). Opposing Shh and Fgf signals initiate nasotemporal patterning of the zebrafish retina. *Development* **142**, 3933-42.

Hinaux, H., Blin, M., Fumey, J., Legendre, L., Heuze, A., Casane, D. and Rétaux, S. (2015). Lens defects in Astyanax mexicanus Cavefish: Evolution of crystallins and a role for alphaA-crystallin. *Dev Neurobiol*, 505-21.

Hinaux, H., Devos, L., Bibliowicz, J., Elipot, Y., Alié, A., Blin, M. and Rétaux, S. (2016). Sensory evolution in blind cavefish is driven by early events during gastrulation and neurulation. *Development* **143**, 4521-4532.

Hinaux, H., Pottin, K., Chalhoub, H., Pere, S., Elipot, Y., Legendre, L. and Rétaux, S. (2011). A developmental staging table for Astyanax mexicanus surface fish and Pachon cavefish. *Zebrafish* **8**, 155-65.

Hinaux, H., Recher, G., Alie, A., Legendre, L., Blin, M. and Retaux, S. (2017). Lens apoptosis in the Astyanax blind cavefish is not triggered by its small size or defects in morphogenesis. *PLoS One* **12**, e0172302.

Hyer, J., Kuhlman, J., Afif, E. and Mikawa, T. (2003). Optic cup morphogenesis requires pre-lens ectoderm but not lens differentiation. *Dev Biol* **259**, 351-63.

Ishikawa, Y., Yoshimoto, M., Yamamoto, N., Ito, H., Yasuda, T., Tokunaga, F., Iigo, M., Wakamatsu, Y. and Ozato, K. (2001). Brain structures of a medaka mutant, el (eyeless), in which eye vesicles do not evaginate. *Brain Behav Evol* **58**, 173-84.

Ivanovitch, K., Cavodeassi, F. and Wilson, S. W. (2013). Precocious acquisition of neuroepithelial character in the eye field underlies the onset of eye morphogenesis. *Dev Cell* **27**, 293-305.

Kawakami, K. (2005). Transposon tools and methods in zebrafish. *Dev Dyn* **234**, 244-54.

Kimura, Y., Hisano, Y., Kawahara, A. and Higashijima, S. (2014). Efficient generation of knock-in transgenic zebrafish carrying reporter/driver genes by CRISPR/Cas9-mediated genome engineering. *Sci Rep* **4**, 6545.

Klaassen, H., Wang, Y., Adamski, K., Rohner, N. and Kowalko, J. E. (2018). CRISPR mutagenesis confirms the role of oca2 in melanin pigmentation in Astyanax mexicanus. *Dev Biol* **441**, 313-318.

Kruse-Bend, R., Rosenthal, J., Quist, T. S., Veien, E. S., Fuhrmann, S., Dorsky, R. I. and Chien, C. B. (2012). Extraocular ectoderm triggers dorsal retinal fate during optic vesicle evagination in zebrafish. *Dev Biol* **371**, 57-65.

Kwan, K. M., Otsuna, H., Kidokoro, H., Carney, K. R., Saijoh, Y. and Chien, C. B. (2012). A complex choreography of cell movements shapes the vertebrate eye. *Development* **139**, 359-72.

Lee, J., Willer, J. R., Willer, G. B., Smith, K., Gregg, R. G. and Gross, J. M. (2008). Zebrafish blowout provides genetic evidence for Patched1-mediated negative regulation of Hedgehog signaling within the proximal optic vesicle of the vertebrate eye. *Dev Biol* **319**, 10-22.

Macdonald, R., Scholes, J., Strahle, U., Brennan, C., Holder, N., Brand, M. and Wilson, S. W. (1997). The Pax protein Noi is required for commissural axon pathway formation in the rostral forebrain. *Development* **124**, 2397-408.

Martinez-Morales, J. R., Rembold, M., Greger, K., Simpson, J. C., Brown, K. E., Quiring, R., Pepperkok, R., Martin-Bermudo, M. D., Himmelbauer, H. and Wittbrodt, J. (2009). ojoplano-mediated basal constriction is essential for optic cup morphogenesis. *Development* **136**, 2165-75.

Maurus, D. and Harris, W. A. (2009). Zic-associated holoprosencephaly: zebrafish Zic1 controls midline formation and forebrain patterning by regulating Nodal, Hedgehog, and retinoic acid signaling. *Genes Dev* **23**, 1461-73.

McGaugh, S. E., Gross, J. B., Aken, B., Blin, M., Borowsky, R., Chalopin, D., Hinaux, H., Jeffery, W. R., Keene, A., Ma, L. et al. (2014). The cavefish genome reveals candidate genes for eye loss. *Nat Commun* **5**, 5307.

764 **Moreno-Marmol, T., Cavodeassi, F. and Bovolenta, P.** (2018). Setting Eyes on the Retinal
765 Pigment Epithelium. *Front Cell Dev Biol* **6**, 145.
766 **Morita, H., Taimatsu, K., Yanagi, K. and Kawahara, A.** (2017). Exogenous gene integration
767 mediated by genome editing technologies in zebrafish. *Bioengineered* **8**, 287-295.
768 **Nicolas-Perez, M., Kuchling, F., Letelier, J., Polvillo, R., Wittbrodt, J. and Martinez-Morales,**
769 **J. R.** (2016). Analysis of cellular behavior and cytoskeletal dynamics reveal a constriction
770 mechanism driving optic cup morphogenesis. *Elife* **5**.
771 **Picker, A. and Brand, M.** (2005). Fgf signals from a novel signaling center determine axial
772 patterning of the prospective neural retina. *Development* **132**, 4951-62.
773 **Picker, A., Cavodeassi, F., Machate, A., Bernauer, S., Hans, S., Abe, G., Kawakami, K., Wilson,**
774 **S. W. and Brand, M.** (2009). Dynamic coupling of pattern formation and morphogenesis in the
775 developing vertebrate retina. *PLoS Biol* **7**, e1000214.
776 **Pottin, K., Hinaux, H. and Rétaux, S.** (2011). Restoring eye size in Astyanax mexicanus blind
777 cavefish embryos through modulation of the Shh and Fgf8 forebrain organising centres.
778 *Development* **138**, 2467-76.
779 **Rembold, M., Loosli, F., Adams, R. J. and Wittbrodt, J.** (2006). Individual cell migration serves
780 as the driving force for optic vesicle evagination. *Science* **313**, 1130-4.
781 **Rétaux, S. and Casane, D.** (2013). Evolution of eye development in the darkness of caves:
782 adaptation, drift, or both? *Evodevo* **4**, 26.
783 **Rétaux, S. and Harris, W. A.** (1996). Engrailed and retinotectal topography. *Trends Neurosci*
784 **19**, 542-6.
785 **Rohr, K. B., Schulte-Merker, S. and Tautz, D.** (1999). Zebrafish zic1 expression in brain and
786 somites is affected by BMP and hedgehog signalling. *Mech Dev* **85**, 147-59.
787 **Sakuta, H., Takahashi, H., Shintani, T., Etani, K., Aoshima, A. and Noda, M.** (2006). Role of
788 bone morphogenic protein 2 in retinal patterning and retinotectal projection. *J Neurosci* **26**,
789 10868-78.
790 **Sanek, N. A., Taylor, A. A., Nyholm, M. K. and Grinblat, Y.** (2009). Zebrafish zic2a patterns the
791 forebrain through modulation of Hedgehog-activated gene expression. *Development* **136**,
792 3791-800.
793 **Schulte, D., Furukawa, T., Peters, M. A., Kozak, C. A. and Cepko, C. L.** (1999). Misexpression
794 of the Emx-related homeobox genes cVax and mVax2 ventralizes the retina and perturbs the
795 retinotectal map. *Neuron* **24**, 541-53.
796 **Shinya, M., Eschbach, C., Clark, M., Lehrach, H. and Furutani-Seiki, M.** (2000). Zebrafish Dkk1,
797 induced by the pre-MBT Wnt signaling, is secreted from the prechordal plate and patterns the
798 anterior neural plate. *Mech Dev* **98**, 3-17.
799 **Sidhaye, J. and Norden, C.** (2017). Concerted action of neuroepithelial basal shrinkage and
800 active epithelial migration ensures efficient optic cup morphogenesis. *Elife* **6**.
801 **Simon, V., Hyacinthe, C. and Retaux, S.** (2019). Breeding behavior in the blind Mexican
802 cavefish and its river-dwelling conspecific. *PLoS One* **14**, e0212591.
803 **Sperry, R. W.** (1963). Chemoaffinity in the Orderly Growth of Nerve Fiber Patterns and
804 Connections. *Proc Natl Acad Sci U S A* **50**, 703-10.
805 **Stahl, B. A., Peuss, R., McDole, B., Kenzior, A., Jaggard, J. B., Gaudenz, K., Krishnan, J.,**
806 **McGaugh, S. E., Duboue, E. R., Keene, A. C. et al.** (2019). Stable transgenesis in Astyanax
807 mexicanus using the Tol2 transposase system. *Dev Dyn*.
808 **Stemmer, M., Schuhmacher, L. N., Foulkes, N. S., Bertolucci, C. and Wittbrodt, J.** (2015).
809 Cavefish eye loss in response to an early block in retinal differentiation progression.
810 *Development* **142**, 743-52.

Stigloher, C., Ninkovic, J., Laplante, M., Geling, A., Tannhauser, B., Topp, S., Kikuta, H., Becker, T. S., Houart, C. and Bally-Cuif, L. (2006). Segregation of telencephalic and eye-field identities inside the zebrafish forebrain territory is controlled by Rx3. *Development* **133**, 2925-35.

Strauss, O. (2018). The retinal pigmented epithelium. *In "The organization of the retina and visual system". Edited by H. Kolb, E Fernandez and R. Nelson. Webvision. University of Utah Health Science Center, Salt Lake City.*

Strickler, A. G., Yamamoto, Y. and Jeffery, W. R. (2001). Early and late changes in Pax6 expression accompany eye degeneration during cavefish development. *Dev Genes Evol* **211**, 138-44.

Take-uchi, M., Clarke, J. D. and Wilson, S. W. (2003). Hedgehog signalling maintains the optic stalk-retinal interface through the regulation of Vax gene activity. *Development* **130**, 955-68.

Thermes, V., Grabher, C., Ristoratore, F., Bourrat, F., Choulika, A., Wittbrodt, J. and Joly, J. S. (2002). I-SceI meganuclease mediates highly efficient transgenesis in fish. *Mech Dev* **118**, 91-8.

Torres-Paz, J., Leclercq, J. and Rétaux, S. (2018). Evolution of gastrulation in Mexican cavefish: heterochronic cell movements and maternal factors. *bioRxiv* **Sept 2018**.

Tropepe, V., Li, S., Dickinson, A., Gamse, J. T. and Sive, H. L. (2006). Identification of a BMP inhibitor-responsive promoter module required for expression of the early neural gene zic1. *Dev Biol* **289**, 517-29.

Varga, Z. M., Wegner, J. and Westerfield, M. (1999). Anterior movement of ventral diencephalic precursors separates the primordial eye field in the neural plate and requires cyclops. *Development* **126**, 5533-46.

Wang, X., Lupo, G., He, R., Barsacchi, G., Harris, W. A. and Liu, Y. (2015). Dorsoventral patterning of the Xenopus eye involves differential temporal changes in the response of optic stalk and retinal progenitors to Hh signalling. *Neural Dev* **10**, 7.

Wilkens, H. (2001). Convergent adaptations to cave life in the Rhamdia laticauda catfish group (Pimelodidae, Teleostei). *Environmental Biology of Fishes* **62**, 251-261.

Winkler, S., Loosli, F., Henrich, T., Wakamatsu, Y. and Wittbrodt, J. (2000). The conditional medaka mutation eyeless uncouples patterning and morphogenesis of the eye. *Development* **127**, 1911-9.

Woo, K. and Fraser, S. E. (1995). Order and coherence in the fate map of the zebrafish nervous system. *Development* **121**, 2595-609.

Woo, K., Shih, J. and Fraser, S. E. (1995). Fate maps of the zebrafish embryo. *Curr Opin Genet Dev* **5**, 439-43.

Yamamoto, Y. and Jeffery, W. R. (2000). Central role for the lens in cave fish eye degeneration. *Science* **289**, 631-3.

Yamamoto, Y., Stock, D. W. and Jeffery, W. R. (2004). Hedgehog signalling controls eye degeneration in blind cavefish. *Nature* **431**, 844-7.

Zhou, C. J., Wang, Y. Z., Yamagami, T., Zhao, T., Song, L. and Wang, K. (2008). Generation of Lrp6 conditional gene-targeting mouse line for modeling and dissecting multiple birth defects/congenital anomalies. *Dev Dyn* **239**, 318-26.

Figures and Legends

858

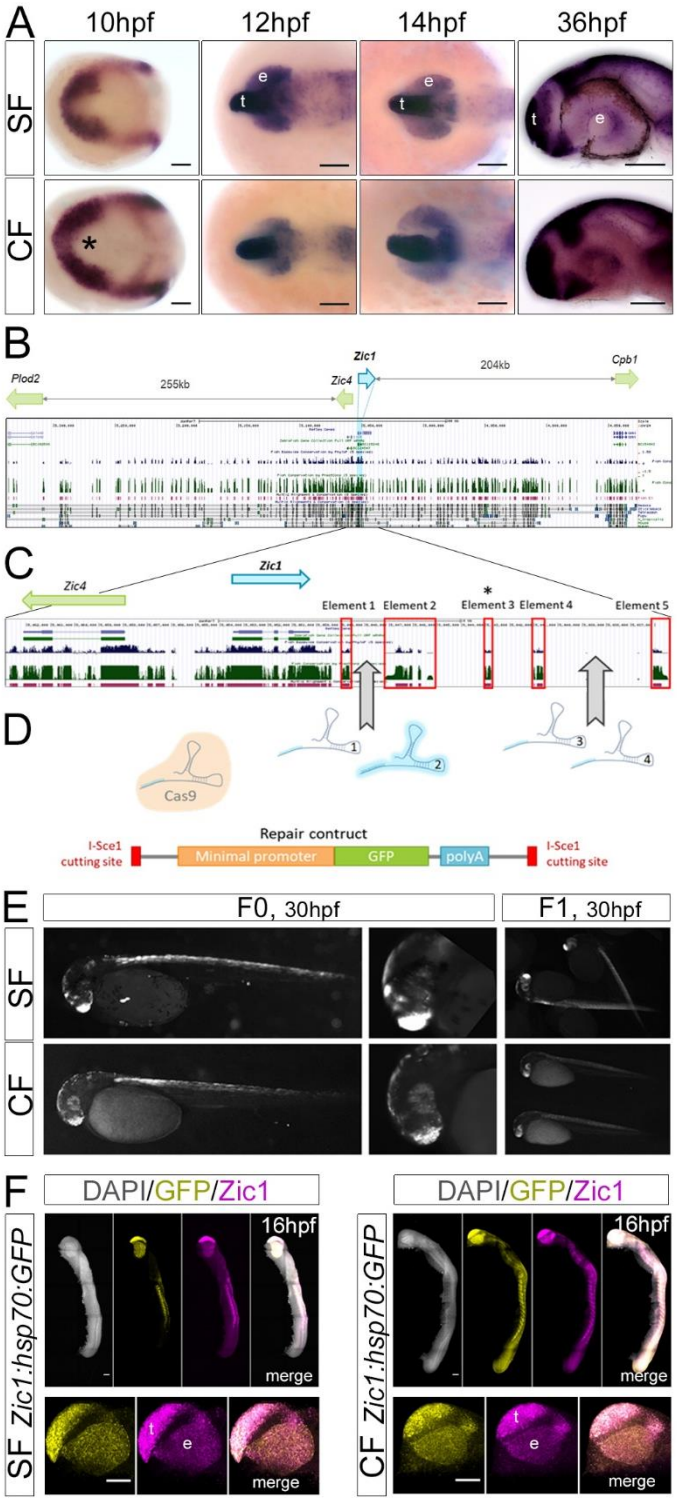

Figure 1

859

860 **Figure 1: establishment of surface fish and cavefish *Zic1:hsp70:GFP* lines.**

861 (A) *Zic1* expression at indicated stages in SF and CF. Anterior is to the left. Dorsal views at 10,
862 12 and 14hpf, lateral views at 36hpf. Asterisk: larger indentation in the CF eyefield.
863 (B) Zebrafish *Zic1* genomic region in UCSC genome browser (2010 assembly). Green blue peaks
864 as well as magenta and black elements correspond to high conservation, showing the
865 complexity of the region.
866 (C) Close-up on *Zic1*. Red boxes highlight conserved elements; element 3 is not conserved in
867 *Astyanax* (asterisk).
868 (C) sgRNA were designed to target the low-conservation regions between elements 1 and 2,
869 and 3 and 4. SgRNA2 (pale blue) efficiently generated cuts. It was co-injected together with
870 the Cas9 protein and the linear repair construct containing a minimal Hsp70 promoter and the
871 GFP.

872 (D) *Zic1-like* GFP fluorescence in mosaic F0s and stable F1s, both for SF and CF.

873 (E) Double-fluorescent *in situ* hybridization at 16hpf for *Zic1* (magenta) and *GFP* (yellow)
874 showing that the transgene recapitulates the endogenous *Zic1* pattern, both for SF and CF
875 lines. The top panels show entire embryos and the bottom panels show close-ups on the head,
876 including the *Zic1*-expressing telencephalon (t) and eye (e). Lateral views.

877 Scale bars=100µm.

878

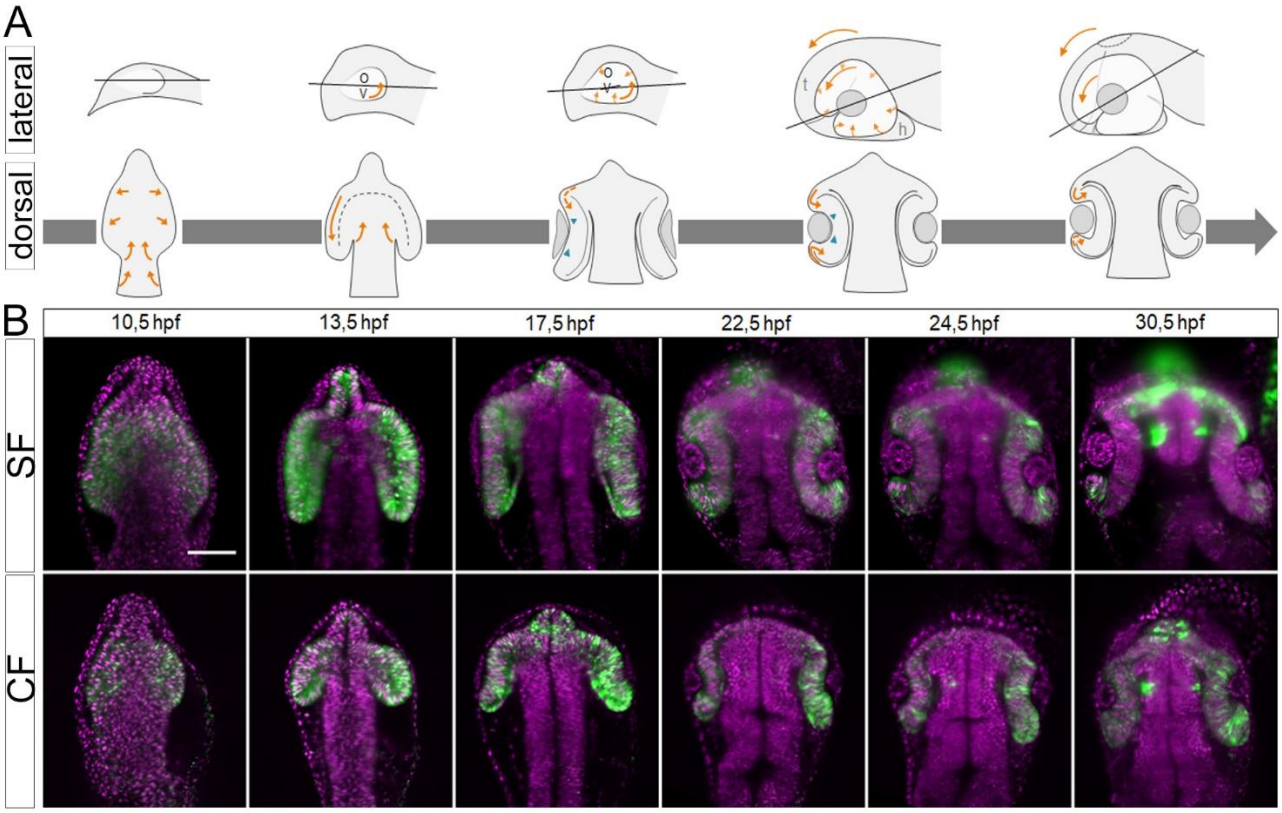

Figure 2

Figure 2: Live imaging of surface fish and cavefish eye morphogenesis.

(A) Schematic drawings of the principal steps of eye morphogenesis in fish, in lateral (top) and dorsal views (bottom). Orange arrows indicate cell and tissue movements; green arrowheads show initiation of basal constriction. The grey line indicates the optical section plane used in the pictures in B, which follows an optic stalk to lens center axis and accompanies the anterior rotation illustrated by the arrows. All subsequent measures were realized on these planes.

(B) Still images of time-lapse acquisitions from 10.5hpf to 30.5hpf on SF and SF *Zic1:hsp70:GFP* lines (green, GFP; magenta, nuclear mCherry). Representative steps of eye morphogenesis illustrating CF/SF differences are shown. Dorsal views, anterior to the top.

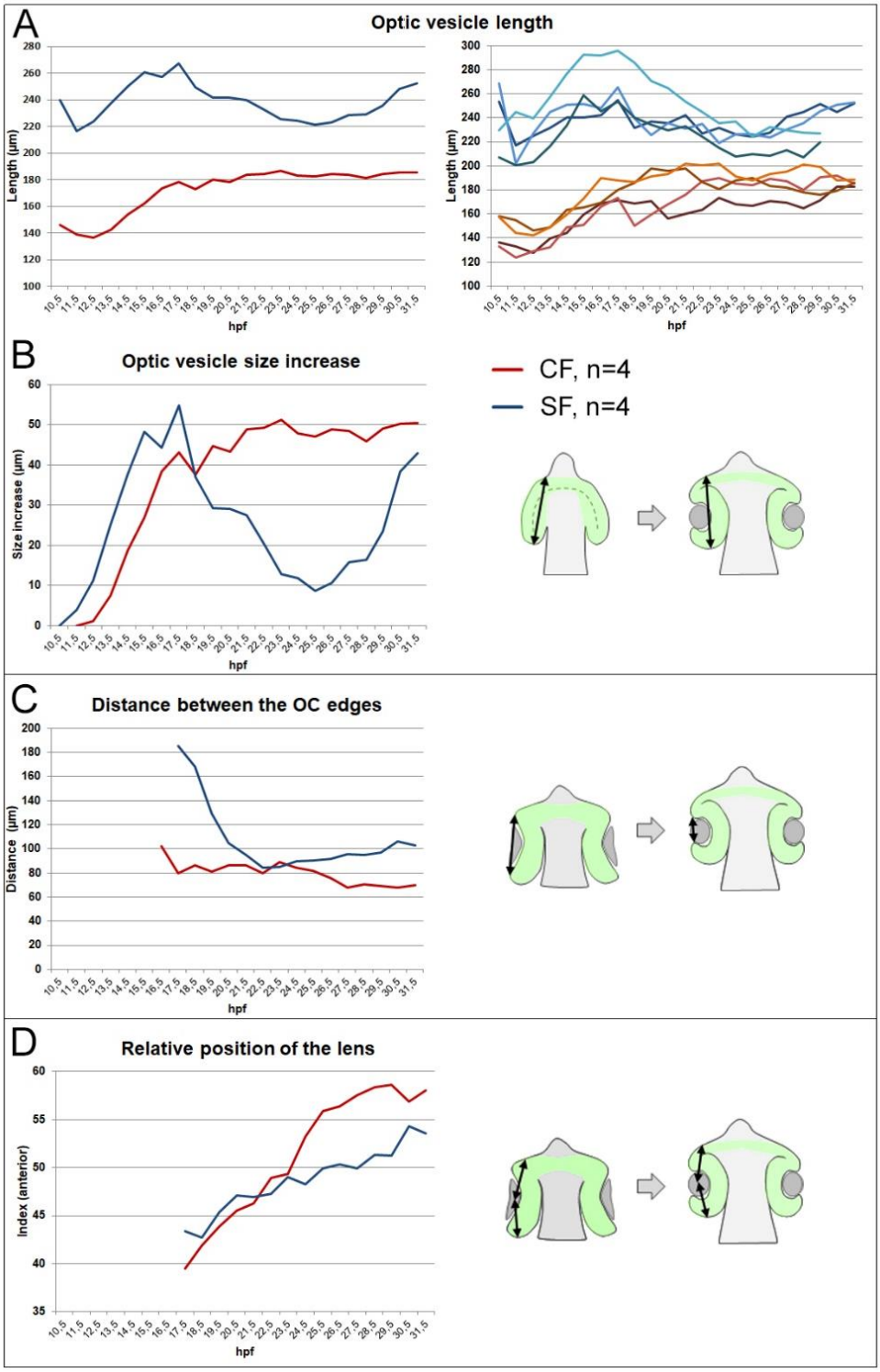

Figure 3

Figure 3: Morphological quantification of eye morphogenesis.

894 Measures are illustrated on the diagrams on the right in each box.

895 (A) Optic vesicle length. The left graph shows the mean of n=4 eyes in each morph (blue, SF;
896 red, CF); the right graph displays the trajectories of individual eyes to show the reproducibility
897 of the results.

898 (B) Optic vesicle size increase.

899 (C) Distance between the two optic cup edges.

900 (D) Position of the lens relative to anterior optic vesicle, showing that the lens is progressively
901 shifted anteriorly between 25hpf and 30hpf.

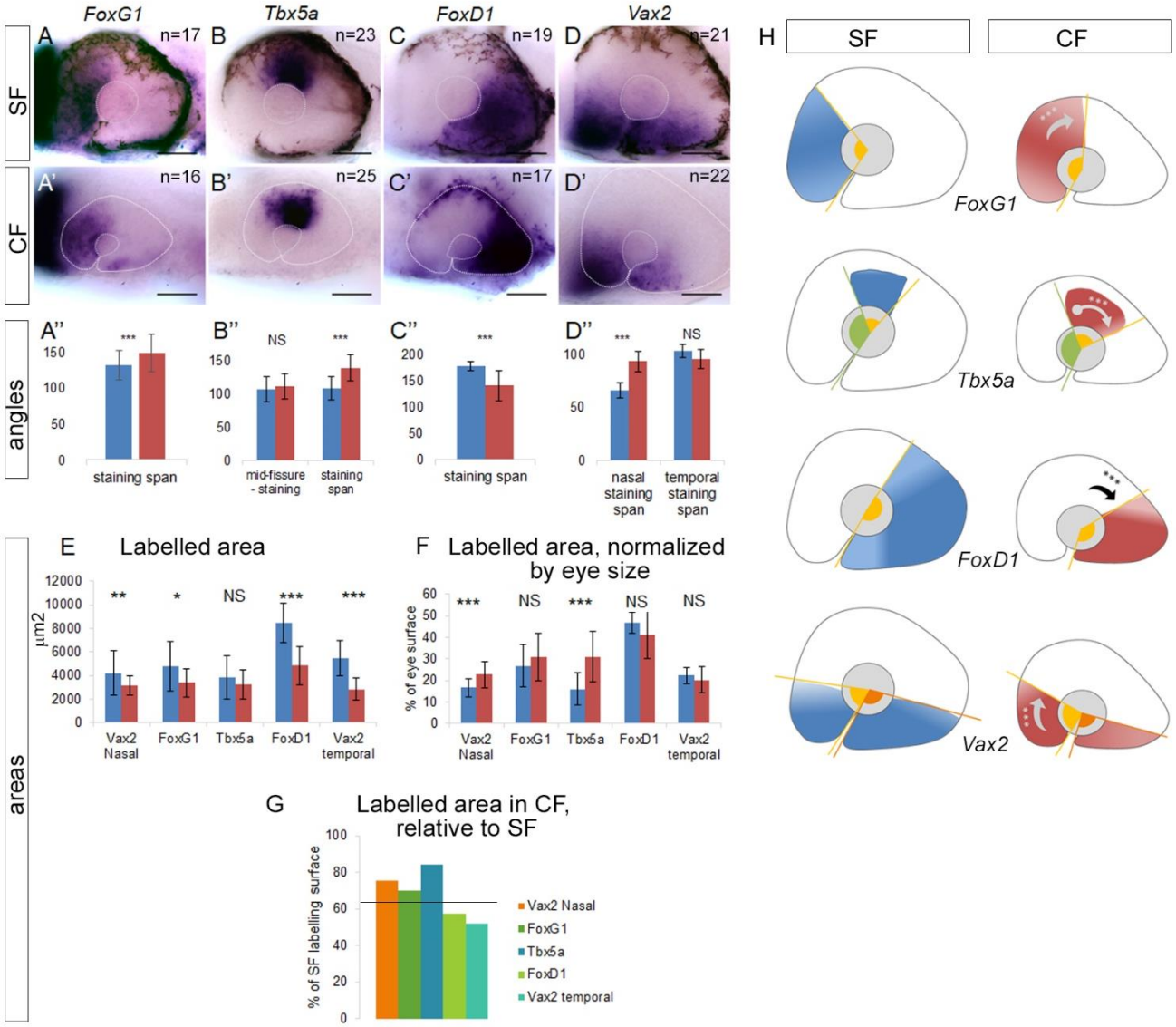

Figure 4

Figure 4: regionalization of the eye.

(A-D') *In situ* hybridization for the indicated markers on 36hpf SF and CF embryos. Sample sizes are indicated.

(A''-D'') Quantification of angles of expression and position with regards to the choroid fissure. All the angles measured are represented in H. SF, blue; CF, red.

(E) Absolute area of expression, in µm^2.

(F) Area of expression normalized by eye size.

(G) Area of expression in CF, expressed as percentage of the expression area in SF. Horizontal line shows that the CF eye area is 64% of the SF eye.

Statistical test: Mann-Whitney; * $p<0.05$; ** $p<0.01$; *** $p<0.001$.

913 (H) Summary diagram of the expression patterns. The angles measured are represented.
914 Expression patterns are represented in blue for SF and red for CF. The angles measured are
915 between the middle of the choroid fissure and the borders of the expression domains.
916

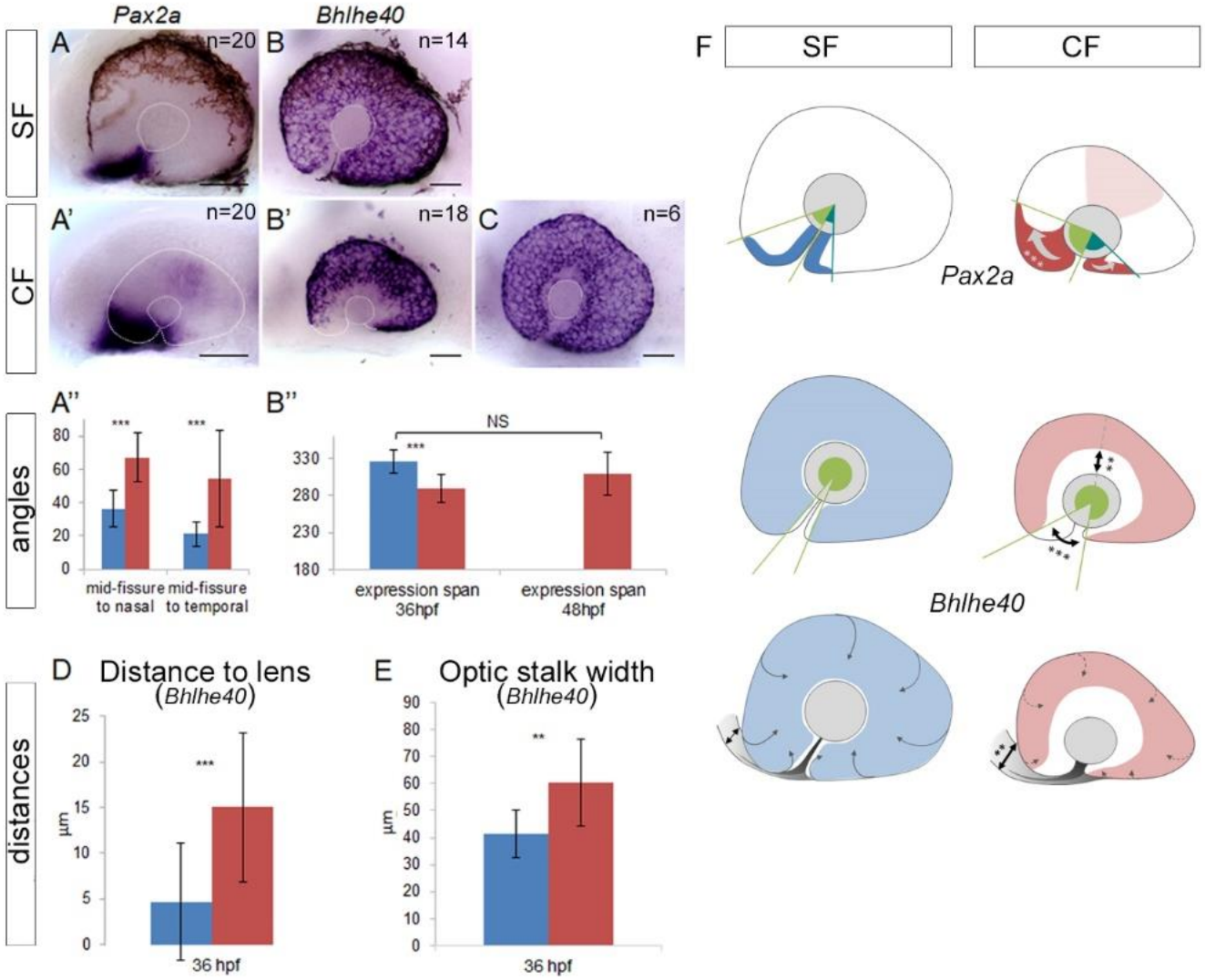

Figure 5

Figure 5: tissue identity.

(A-B') In *situ* hybridization for the indicated markers on 36hpf SF and CF embryos. (C) *Bhlhe40* expression in 48hpf CF. Sample sizes are indicated.

(A'') Angle between the optic fissure and the limit of *Pax2a* domain (see F for angles measured).

(B'') Angles of *Bhlhe40* expression at 36 and 48hpf.

(D) Distance between *Bhlhe40*-expressing cells and the lens at 36hpf.

(E) Width of the *Bhlhe40* expression gap at the back of the eye. SF, blue; CF, red.

Statistical test: Mann-Whitney; * $p<0.05$; ** $p<0.01$; *** $p<0.001$.

(F) Summary diagram of expression patterns. Angles measured are represented.

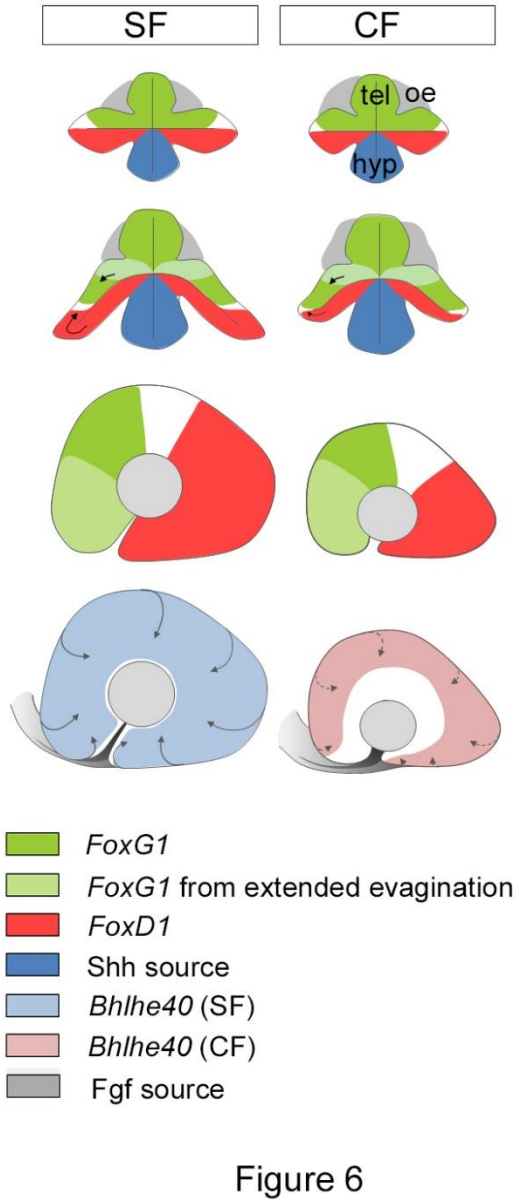

Figure 6: summary and hypothetical scenario for cavefish eye development defects. Combining data from live imaging and gene expression patterns, we propose that the small size of the optic vesicles, correctly patterned, explains the decrease in temporal quadrant size. Unaltered extended evagination movements bring new cells into the prospective nasal retina, partially rescuing its size (pale green). Finally, the expansion of the RPE to engulf the retina which is concomitant with the rim movement is delayed, leaving the optic stalk wide and optic fissure margins away from each other.

oe, olfactory epithelium; tel, telencephalon; hyp, hypothalamus.

Supplemental Figures and Legends

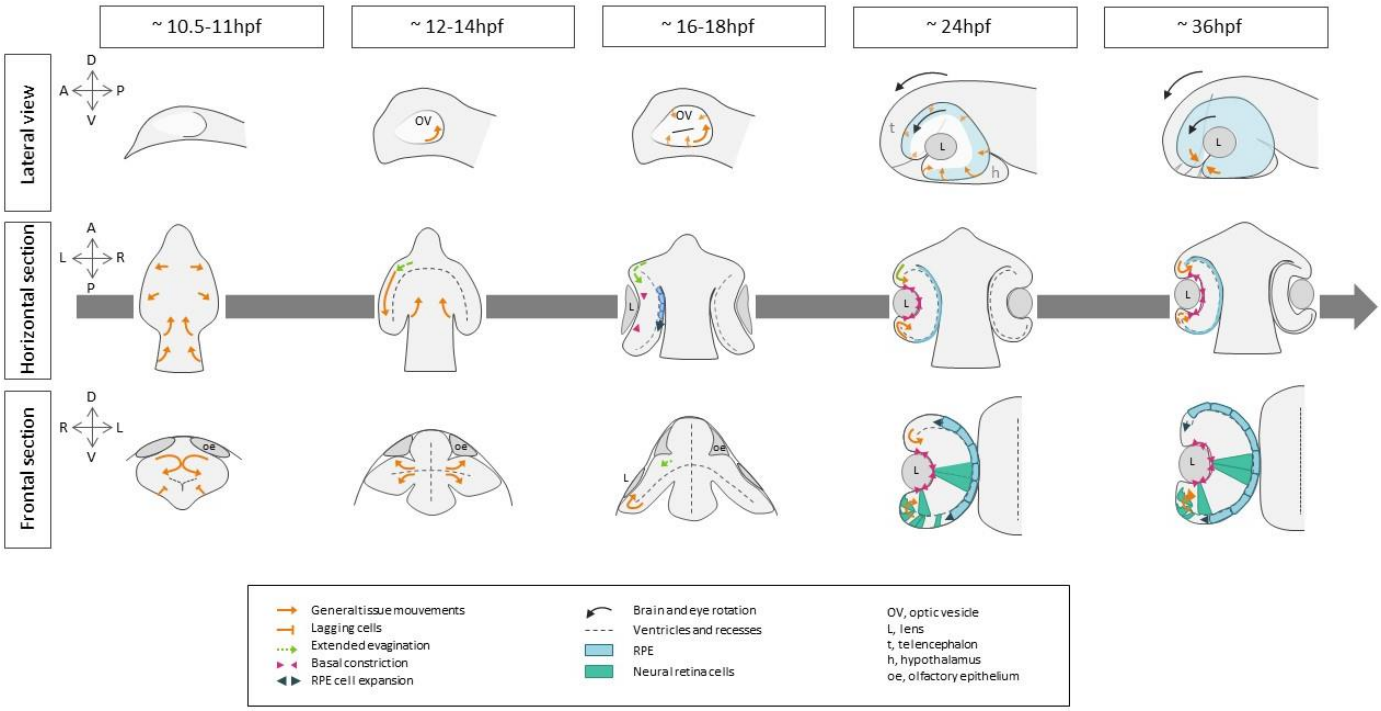

Supplemental Figure 1: eye morphogenesis in fish.

Schemes depicting the principal steps of eye morphogenesis in fish models, summarized from the available literature cited in Introduction.

Stages and orientations are indicated.

Orange arrows show general cell and tissue movements.

Black arrows show the anterior-wise rotation of the eye and brain.

Green arrows show the contribution of extended evagination.

Pink arrowhead show cellular basal constriction.

The blue color depicts the RPE cells, while the green color depicts retina neuroepithelium cells changing shape.

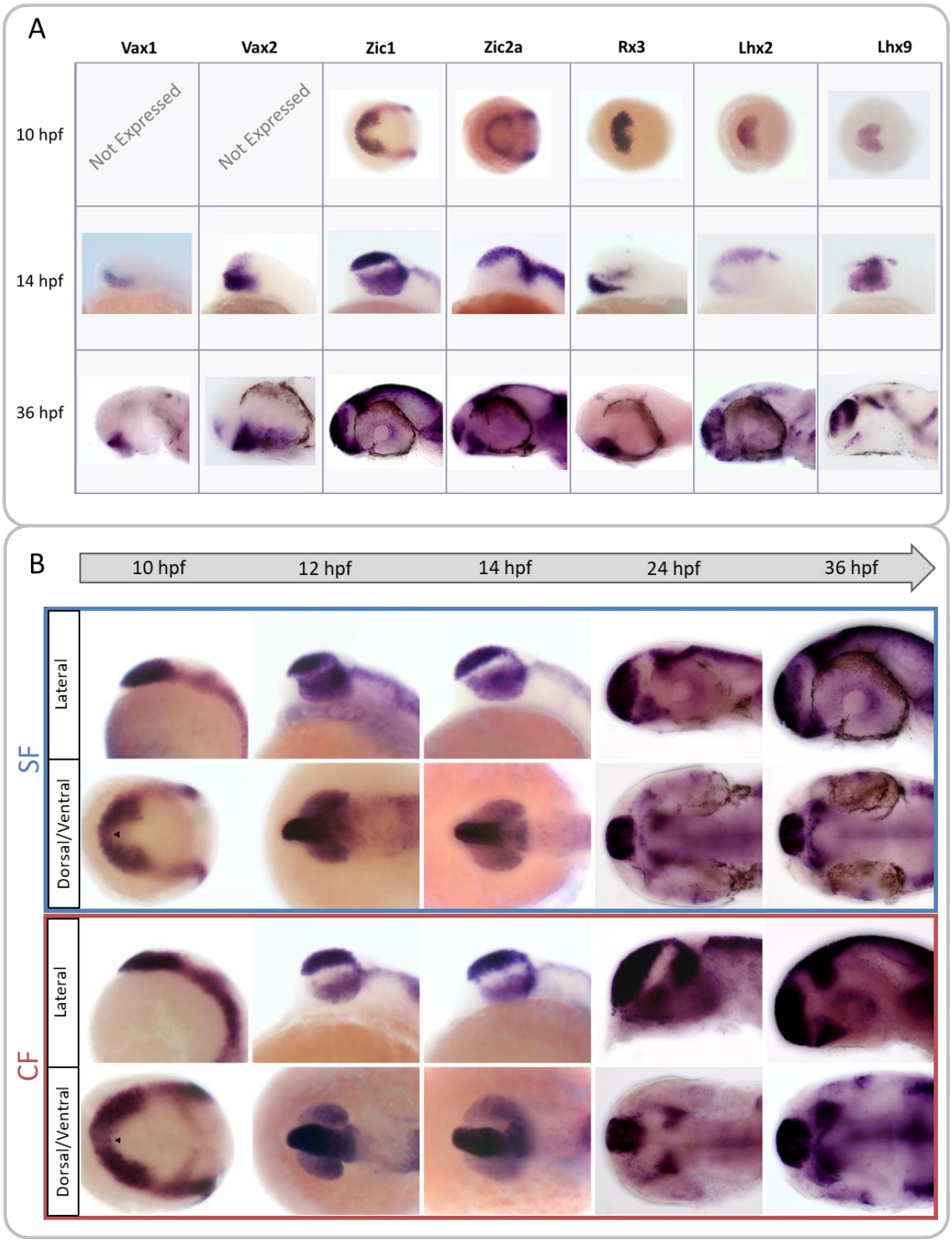

954

955 **Supplemental Figure 2: choosing a candidate gene for transgenesis.**

956 (A) Mini-screen of candidate genes by *in situ* hybridization at different stages of interest on

957 surface fish embryos (anterior is to the left). Dorsal views at 10hpf; lateral views at 14hpf and

958 36hpf. The eyes were dissected out for *Vax1* and *Lhx9* (as no eye expression was detected for
959 either of them) to allow better visibility of the inner tissue.
960 (B) Detailled analysis of *Zic1* expression pattern at 5 different stages in surface (SF) and
961 cavefish (CF). Anterior is to the left, at 10, 12 and 14hpf, bottom pictures are taken in dorsal
962 view; at 24 and 36hpf, bottom picture are taken in ventral views. Arrowheads indicate an
963 indentation in the eyefield.

964 ***Description of expression patterns:***

965 *Vax1* expression was detectable from 12hpf in the presumptive ORR (between the optic
966 vesicles) and additionally in the dorsal hypothalamus (according to brain axis (Puelles &
967 Rubenstein, 2015), closest to the ORR) and quite faintly in the ventral telencephalon.

968 *Vax2* expression was very similar to *Vax1* both in terms of onset of expression and pattern,
969 with the addition of the ventral quadrant of the eye. Although *Vax2* had a very interesting
970 ventral pattern, we discarded it as a candidate for transgenesis for its expression onset was
971 very late. Moreover, in *Vax2* enhancer trap zebrafish line (Kawakami Laboratory), the GFP
972 fluorescence is only visible at 18hpf (personal observation, data not shown).

973 *Rx3* expression showed a typical eyefield expression pattern at 10hpf but progressively faded
974 away during optic vesicle stages and was finally not expressed anymore at 24hpf. Conversely,
975 an anterior and ventral expression in the presumptive hypothalamus was detectable from
976 12hpf and remained throughout the stages examined. At 36hpf, it was clear that only the
977 dorsal half of the hypothalamus, closest to the ORR, was labelled. Due to the rapid fading of
978 its optic vesicle expression, we did not consider *Rx3* as a valid candidate.

979 *Lhx2* and *Lhx9* were both already known to be expressed in the eyefield at neural plate stages
980 in *Astyanax* (Pottin et al., 2011). *Lhx2* expression showed very dim expression, if any, in the
981 optic vesicles at 12 and 14hpf but was expressed both in the prospective telencephalon and
982 more faintly in the prospective hypothalamus. Later on at 36hpf, *Lhx2* was expressed strongly
983 in the telencephalon and the olfactory epithelia; lighter expression was also visible in the ORR,
984 hypothalamus and sometimes eyes. Additional expression in the pineal, optic tectum and in
985 the hindbrain was also present.

986 *Lhx9* staining was strong in the optic vesicles at 12hpf (during evagination) and slightly lighter
987 at 14hpf. Moreover dorsal and ventral lateral labelling at the border of the neural keel and the

988 optic vesicles appeared, possibly prefiguring respectively the strong telencephalic staining
989 visible at 24 and 36hpf and the hypothalamic cluster at the limit of the ORR already described
990 in a previous publication (Alié et al., 2018). At these late stages, we could not detect *Lhx9*
991 expression in the eye anymore. Salt and pepper staining was visible in the olfactory epithelia;
992 a band of expression outlining the optic tectum and lateral discrete marks in the hindbrain
993 were present. We did not choose *Lhx2* or *Lhx9* because of the rapid decay of their eye
994 expression.

995 At 10hpf, *Zic2a* was expressed at the border of the neural plate and almost entirely
996 surrounding the eyefield except for a medial posterior gap. Faint staining in the bilateral
997 eyefield could also be seen on some embryos. At 12 and 14hpf, there was a strong *Zic2a*
998 expression in the telencephalon and a faint staining in the eye or distal part of the eye could
999 often be seen. Strong staining was generally visible throughout the dorsal-most brain. At
1000 24hpf, *Zic2a* expression remained strong in the telencephalon and was also now strongly
1001 visible at the border of the eye, in the ORR or optic stalk but without reaching the midline.
1002 Faint staining in the eye remained. At 36hpf, the expression pattern was similar, with the
1003 ORR/optic stalk staining reaching much closer to the midline. The eye expression was now
1004 more focused around the lens, probably in the CMZ. Roof plate staining persisted throughout
1005 development. Because *Zic2a* was never strongly expressed in the eye, we did not favour it as
1006 a candidate for transgenesis.

1007 *Zic1* was strongly expressed at 10hpf in the neural plate border and in the anterior neural
1008 plate, at the level of the eyefield. At 12 and 14hpf, *Zic1* expression was consistently found in
1009 the optic vesicles and between them (prospective ORR and optic stalk). A strong staining was
1010 also present throughout the telencephalon. More posteriorly, the roof plate of the midbrain
1011 and hindbrain was stained. The somites were also labelled. The pattern was very similar at
1012 24hpf and 36hpf with a strong telencephalic expression and a milder ORR expression (mainly
1013 laterally and posterior to the optic recess)/optic stalk and eye staining (widely around the
1014 lens). Roof plate and somites expression remained. Even though its pattern of expression was
1015 complex and encompassed a region wider than the optic region of interest, *Zic1* was chosen
1016 for transgenesis due to its early and persistent expression throughout the eye and the
1017 ORR/optic stalk regions.

1018

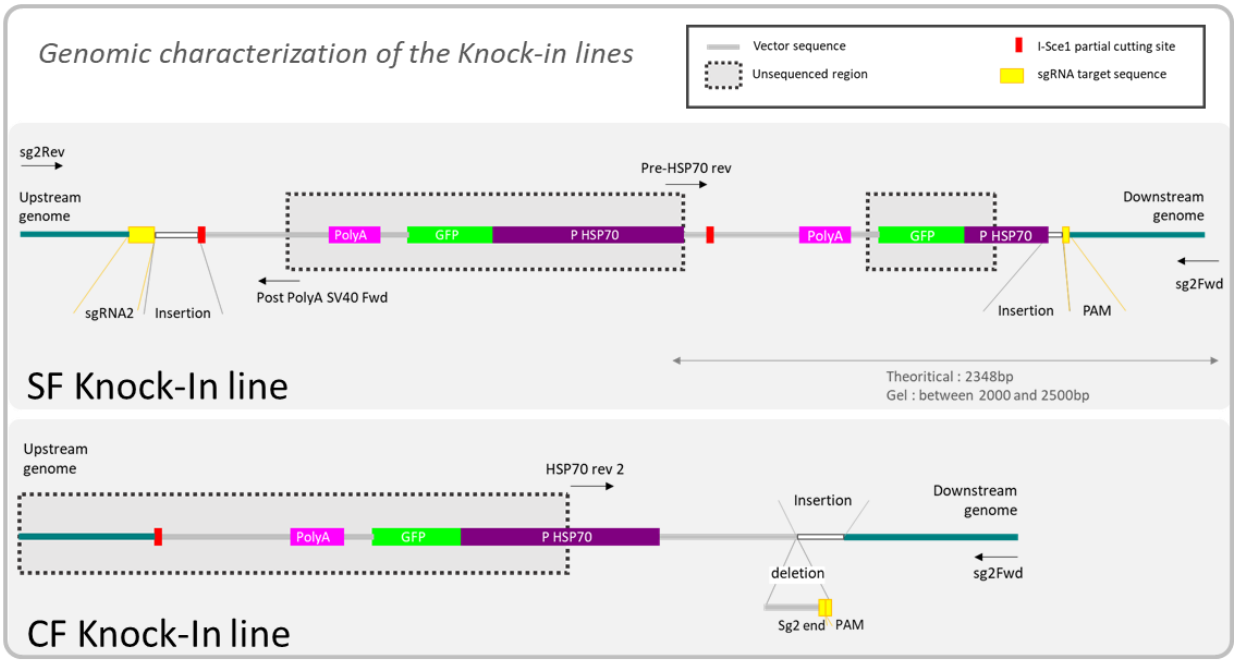

Supplemental Figure 3: genomic characterization of the Knock-in lines.

Knock-In insertions, based on partial sequencing. Dotted boxes indicate un-sequenced regions, leaving uncertainties. For example, in the surface fish line, there is at least a partial insertion of the repair construct, containing a truncated Hsp70 promoter and at least another insert in the same direction (but potentially several). Of note, the surrounding genomic region is very rich in T and A (GC content around 35%) with many repeats, making PCRs sometimes challenging.

The data show that for both lines the transgenes are inserted at the correct targeted site.

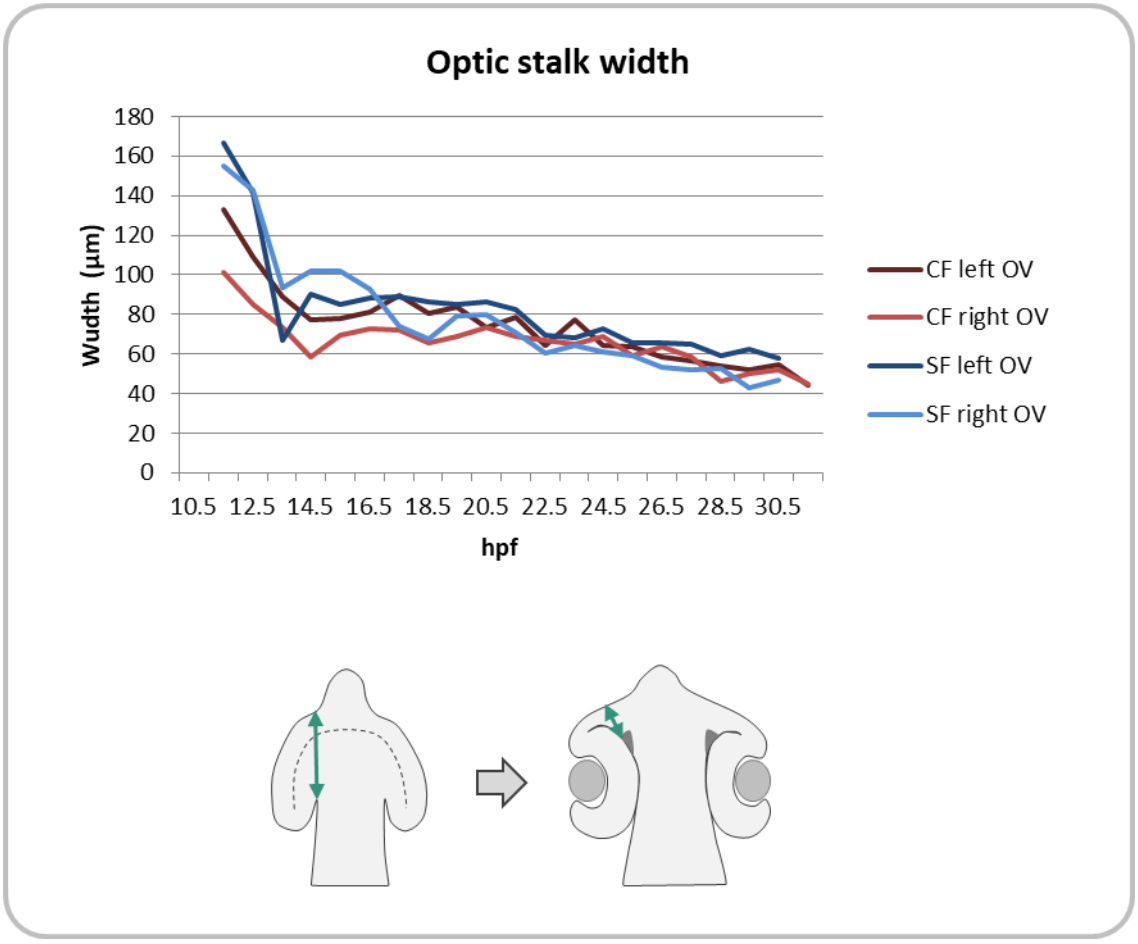

Supplemental Figure 4: optic stalk width.

The size of the optic stalk (in a wide meaning: the connection between the optic vesicle and the neural tube) is smaller in cavefish during early development due to the smaller size of the optic vesicles but rapidly becomes indistinguishable from the optic stalk of the surface fish.

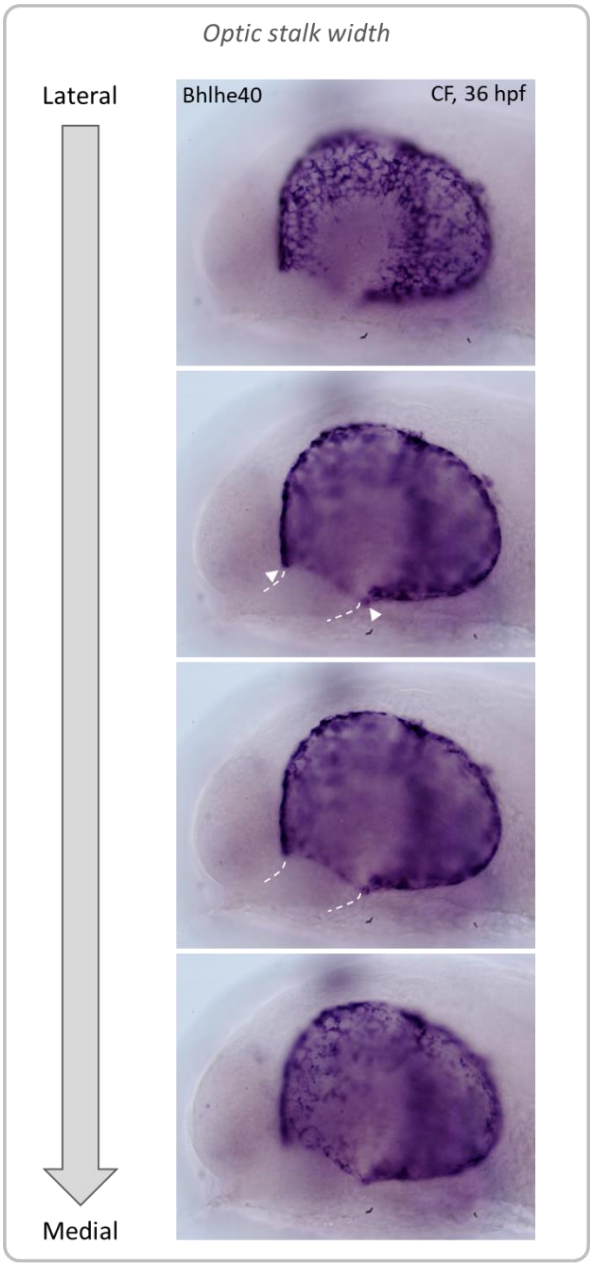

Supplemental Figure 5: illustration of the gap of *Bhlhe40* staining, which we interpret as the optic stalk width.

Different focuses of the same embryo, from lateral to medial on the felt eye. Arrowheads indicate the limits of the staining gap we measured. Dotted lines show the exit trajectory of the optic stalk.

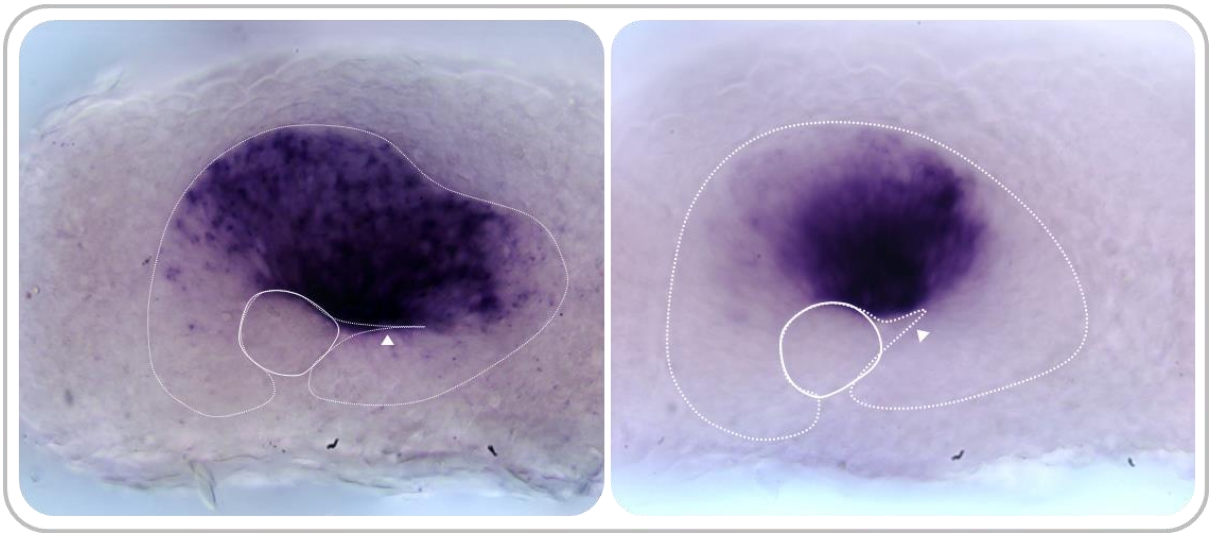

Supplemental Figure 6: retinal folds in cavefish.

Illustration of the retina folds sometimes observed in cavefish: an “extreme case” on the left and a more moderate case on the right. 36hpf cavefish embryos, mounted laterally, anterior is to the left.

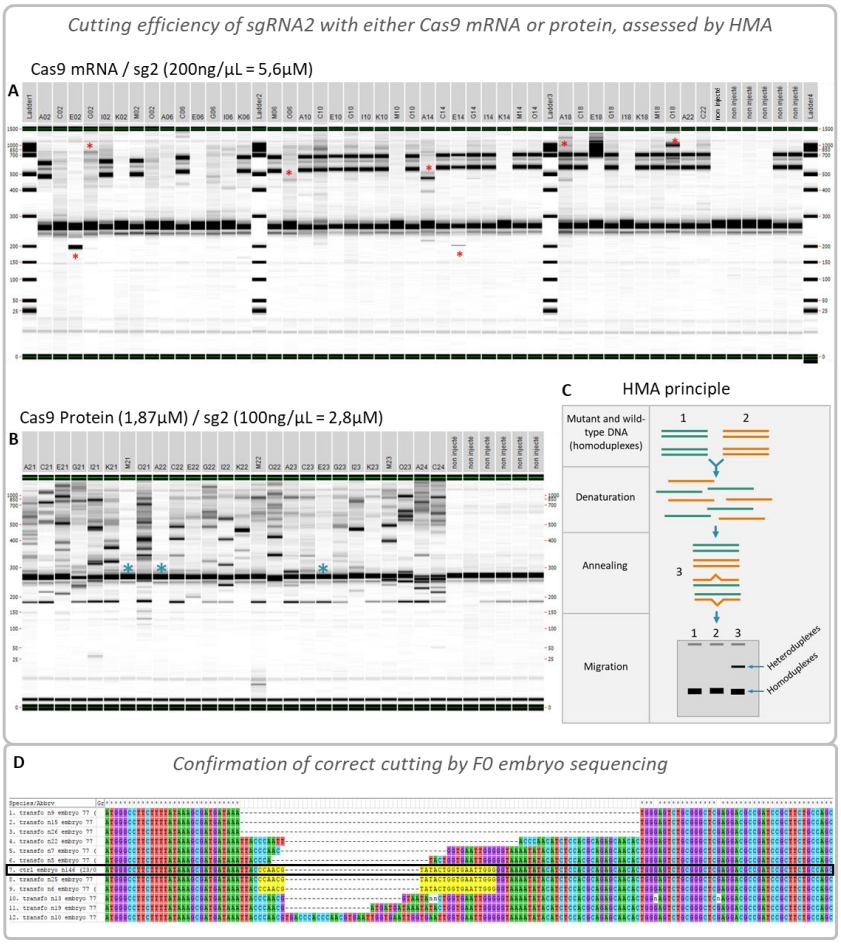

Supplemental Figure 7: cutting efficiency of sgRNA 2

(A) Assessment of sgRNA 2 cutting efficiency when injected with Cas9 mRNA by heteroduplex mobility assay (HMA, explained in (C)). Each column is an individual F0 embryo. Embryos with strong additional bands are labelled with a red asterisk; additional light bands can be seen in several individuals, indicating cuts and imprecise repairs. Note that the 2 heavy bands seen on many embryos are also present in some of the un-injected controls (the 6 columns on the right) indicating a polymorphism in this region in the wild-type fish (not on the sgRNA target sequence).

(B) Assessment of sgRNA 2 cutting efficiency when injected with Cas9 protein, note the strong presence of additional band compared to the 6 control embryos on the right. Embryos without any visible cuts are labelled with a blue asterisk. Additional bands are seen much more frequently and are much more important than with the Cas9 mRNA injection, probably indicating more frequent but also more precocious cut and repair events in the embryo, so that many cells share the same sequence.

1069 (C) Principle of the heteroduplex mobility assay: in an electrophoresis, heteroduplexes are
1070 slowed down compared to homoduplexes so that they form additional bands that can be seen
1071 even if the polymorphism is only a single substitution. In short, the DNA fragments are
1072 denatured and renatured to form heteroduplexes. An electrophoresis is then performed (here
1073 with a LabChip, PerkinElmer) to detect the presence of polymorphism.
1074 (D) Different cutting and repair events in a single injected embryo. A PCR was performed on
1075 one injected embryo (100ng/µL sgRNA2, Cas9mRNA) around the sgRNA2 target site and the
1076 product was cloned into pGEM-T Esay (Promega) and transformed into One shot TOP10
1077 competent bacteria (Thermo Fischer). Plasmidic preparations from individual colonies were
1078 then sequenced. Various sequences were obtained, evidencing different cut and repair events
1079 in one single embryo. sgRNA2 target sequence is highlighted in yellow whenever intact. This
1080 F0 fish harbours both insertions and deletions around the cutting site of sgRNA2. A non-
1081 injected control fish sequence is included, outlined in black.
1082
1083